

# 1 Accretion, retreat and transgression of coastal wetlands 2 experiencing sea-level rise

3 Angelo Breda<sup>1</sup>, Patricia M. Saco<sup>1\*</sup>, Steven G. Sandi<sup>1</sup>, Neil Saintilan<sup>2</sup>, Gerardo Riccardi<sup>3</sup>, José  
4 F. Rodríguez<sup>1\*</sup>

5 <sup>1</sup> School of Engineering and Centre for Water Security and Environmental Sustainability, The University of  
6 Newcastle, Callaghan 2308, Australia

7 <sup>2</sup> Department of Environmental Sciences, Macquarie University, North Ryde 2109, Australia

8 <sup>3</sup> Department of Hydraulics and Research Council of National University of Rosario, Rosario 2000, Argentina

9 *Correspondence to:* Patricia M. Saco (patricia.saco@newcastle.edu.au), José F. Rodríguez  
10 (jose.rodriguez@newcastle.edu.au)

11 **Abstract.** The vulnerability of coastal wetlands to future sea-level rise (SLR) has been extensively studied in  
12 recent years, and models of coastal wetland evolution have been developed to assess and quantify the expected  
13 impacts. Coastal wetlands respond to SLR by vertical accretion and landward migration. Wetlands accrete due to  
14 their capacity to trap sediments and to incorporate dead leaves, branches stems and roots into the soil, and they  
15 migrate driven by the preferred inundation conditions in terms of salinity and oxygen availability. Accretion and  
16 migration strongly interact and they both depend on water flow and sediment distribution within the wetland, so  
17 wetlands under the same external flow and sediment forcing but with different configurations will respond  
18 differently to SLR. Analyses of wetland response to SLR that do not incorporate realistic consideration of flow  
19 and sediment distribution, like the bathtub approach, are likely to result in poor estimates of wetland resilience.  
20 Here, we investigate how accretion and migration processes affect wetland response to SLR using a computational  
21 framework that includes all relevant hydrodynamic and sediment transport mechanisms that affect vegetation and  
22 landscape dynamics, and it is efficient enough computationally to allow the simulation of long time periods. Our  
23 framework incorporates two vegetation species, mangrove and saltmarsh, and accounts for the effects of natural  
24 and manmade features like inner channels, embankments and flow constrictions due to culverts. We apply our  
25 model to simplified domains that represent four different settings found in coastal wetlands, including a case of a  
26 tidal flat free from obstructions or drainage features and three other cases incorporating an inner channel, an  
27 embankment with a culvert, and a combination of inner channel, embankment and culvert. We use conditions  
28 typical of SE Australia in terms of vegetation, tidal range and sediment load, but we also analyse situations with  
29 three times the sediment load to assess the potential of biophysical feedbacks to produce increased accretion rates.  
30 We find that all wetland settings are unable to cope with SLR and disappear by the end of the century, even for  
31 the case of increased sediment load. Wetlands with good drainage that improves tidal flushing are more resilient  
32 than wetlands with obstacles that result in tidal attenuation, and can delay wetland submergence by 20 years.  
33 Results from a bathtub model reveals systematic overprediction of wetland resilience to SLR: by the end of the  
34 century, half of the wetland survives with a typical sediment load, while the entire wetland survives with increased  
35 sediment load.

36  
37 *Keywords:* coastal wetlands, sea-level rise, accretion, migration, hydrodynamic model, sediment transport model,  
38 mangrove, saltmarsh.

## 39 1 Introduction

40 The vulnerability of coastal wetlands to future sea-level rise has been extensively studied in recent years, and  
41 models of coastal wetland evolution have been developed to assess and quantify the expected impacts (Alizad et  
42 al., 2016b; Belliard et al., 2016; Clough et al., 2016; D'Alpaos et al., 2011; Fagherazzi et al., 2012; Kirwan and  
43 Megonigal, 2013; Krauss et al., 2010; Lovelock et al., 2015b; Mogensen and Rogers, 2018; Rodriguez et al.,  
44 2017; Rogers et al., 2012; Schuerch et al., 2018). Predictions vary widely, which is not surprising given the  
45 complexity of the processes involved and the practical challenges associated with representing interactions at a  
46 variety of spatial and temporal scales. Coastal wetlands respond to SLR by vertical accretion and landward  
47 migration. Vertical accretion occurs due to the capacity of wetland vegetation to trap sediments and to incorporate  
48 dead leaves, branches stems and roots into the soil, building up their vertical elevation and counteracting  
49 submergence due to SLR. Landward migration is driven by the preferred inundation conditions of wetland  
50 vegetation, which is continuously moving up the wetland slope due to SLR. These two main processes interact,  
51 but they also integrate a number of biophysical exchanges that occur smaller scales. Accretion is a function of  
52 many other variables like the tidal regime, sediment availability and type of vegetation (Fagherazzi et al.,  
53 2012; Lovelock et al., 2015a). Vegetation preference is dictated by salinity, oxygen availability and the presence  
54 of phytotoxins in the soil (Bilskie et al., 2016; Crase et al., 2013).

55 Studies show that different modelling approaches used to address the interaction between these variables may lead  
56 to divergent results (Alizad et al., 2016a; Rogers et al., 2012). For the sake of simplicity, some previous studies  
57 have adopted an approach where water levels throughout the wetland remain the same as those observed at the  
58 ~~entrance~~inlet, i.e. the bathtub approach (D'Alpaos et al., 2011; Kirwan and Guntenspergen, 2010; Kirwan et al.,  
59 2010; Kirwan et al., 2016a; Lovelock et al., 2015b). Most of these bathtub model results show that vegetation in  
60 coastal areas can produce accretion rates similar to sea-level rise predictions, therefore maintaining their elevation  
61 in the tidal prism, except when tidal range and sediment supply are very low. However, the projections of coastal  
62 wetland resilience under high rates of SLR appears to be at odds with ~~palaeo~~palco-environmental reconstructions  
63 of wetland responses to rising seas during the early Holocene (Horton et al., 2018; Saintilan et al., 2020). One  
64 explanation of this discrepancy is that models fail to reproduce the flow attenuation caused by the friction induced  
65 by substrate cover and specific wetland features like inner channels, embankments and flow constrictions (Hunt  
66 et al., 2015) and its effects on sediment availability, which may result in overestimation of wetland accretion rates  
67 (Rodriguez et al., 2017). Bathtub models do not provide information on flow discharges or velocities, so they need  
68 an independent specification of sediment concentration.

69 On the other hand, more detailed description of hydrodynamic and sediment transport mechanisms can be  
70 incorporated into the computations of wetland dynamics using conventional two or three dimensional flow and  
71 sediment transport models (Ganju et al., 2015; Lalimi et al., 2020; Temmerman et al., 2005). A detailed description  
72 of flow and sediment transport processes can potentially result in a better estimation of wetland dynamics  
73 including accretion and migration processes, but implementation can be seriously limited by computational cost  
74 and data availability (Beudin et al., 2017).

75 Here, we investigate how accretion and migration processes affect wetland response to SLR using a computational  
76 framework that ~~includes-integrates all-relevant~~detailed hydrodynamic and sediment transport mechanisms that  
77 affect vegetation and landscape dynamics, ~~yet it and that~~ is efficient enough to allow the simulation of long time  
78 periods. The framework consists of a fast-performance quasi-2D hydrodynamic model (Riccardi, 2000; Rodriguez

79 et al., 2017) that we have extensively tested in wetlands (Rodriguez et al., 2017;Saco et al., 2019;Sandi et al.,  
80 2018;Sandi et al., 2019;Sandi et al., 2020a;Sandi et al., 2020b) and a sediment advection transport model (Garcia  
81 et al., 2015) that we couple with vegetation formulations for preference to tidal conditions to obtain realistic  
82 predictions of wetland accretion and migration under SLR. Our framework incorporates two vegetation species,  
83 mangrove and saltmarsh, and accounts for the effects of manmade features like inner channels, embankments and  
84 flow constrictions due to culverts. We apply our model to simplified domains that represent distinct areas within  
85 a real wetland, in which we are able to characterise the effects of particular natural and manmade wetland features  
86 like vegetation types, culverts, embankments and channels.

87 Coastal wetlands are found over a broad spectrum of geomorphological settings (Woodroffe et al., 2016) and  
88 under a diverse set of anthropogenic interventions (Temmerman and Kirwan, 2015). While our results strictly  
89 apply to areas ~~of our~~in a particular wetland in Southeast Australia, each of our selected domains focusses on  
90 ~~particular-specific~~ geomorphological characteristics that may also be present in other wetlands worldwide. We  
91 study wetland evolution on domains with no drainage network or manmade structures, which is relevant for some  
92 low-tide wetland environments where no human intervention has occurred (Leong et al., 2018;Oliver et al.,  
93 2012;Tabak et al., 2016). We simulate the dynamics of internal channels, which can provide insight on wetlands  
94 studies with strong influence of natural channels (Reef et al., 2018;Silvestri et al., 2005) or manmade drainage  
95 channels (Manda et al., 2014). We carry-out ~~experiments~~simulations with embankments and culverts representing  
96 flood sheltered environments, which can resemble intentional flood attenuation works for coastal protection (Van  
97 Loon-Steensma et al., 2015) or unintentional flood attenuation as the result of roads, tracks, pipes and other  
98 infrastructure typical of heavily human-occupied coasts (Kirwan and Megonigal, 2013;Rodriguez et al.,  
99 2017;Temmerman et al., 2003).

100 Also, and in order to make our results more widely relevant, we analyse the sensitivity of our predictions  
101 to the sediment load coming into the wetland by including sediment-poor and sediment-rich simulations. The  
102 incoming sediment load has been proposed as one of the main factor influencing the resilience of coastal wetlands  
103 to SLR (Lovelock et al., 2015a;Schuerch et al., 2018) and is one of the components of predictive wetland evolution  
104 models with more uncertainty, due both to our limited understanding of sediment-flow-vegetation processes and  
105 our inability to predict sediment loads in a changing future.

## 106 **2 Experimental design and methods**

### 107 **2.1 Design of simulations**

108 The flow in tidal wetlands can be quite complex because of the interaction of the tidal flow with natural and  
109 manmade features like vegetation, topography, channels, culverts and embankments. For that reason, results for  
110 a particular wetland may have limited applicability to another wetland with different features. In this contribution,  
111 we analyse some of the most common features of wetlands in isolation in order to gain a better understanding of  
112 the contribution of each feature to the overall wetland response, and how it influences the response to sea-level  
113 rise. For that purpose, we study the response of wetlands with limited complexity using a state of the art  
114 ecogeomorphological model on four hypothetical tidal flats that characterise specific areas of a typical SE  
115 Australian coastal wetland that we have studied before (Fig.1a,b) (Rodriguez et al., 2017). Simulation 1 uses a  
116 bathhtub approach over a consistently sloping tidal flat initially vegetated by mangrove, saltmarsh and freshwater

117 vegetation (Fig. 1c), in which water levels are considered uniform over the domain and no special features are  
118 taken into Experimentaccount. In contrast, for Simulations 2 to 5, water levels are calculated with the  
119 hydrodynamic model, which allows for the inclusion of attenuation effects from vegetation and special features.  
120 Simulation 2 considers a vegetatedeconsistently sloping tidal flat with no special features, initially vegetated by  
121 mangrove, saltmarsh and freshwater vegetation, ExperimentSimulation 3 incorporates a drainage channel 0.4 m  
122 deep and 5 m wide to the vegetated tidal flat, ExperimentSimulation 4 includes an embankment with a culvert  
123 (0.4-8 m wide and 0.5 m tall) in the middle of the vegetated flat, and ExperimentSimulation 5 combines both a  
124 drainage channel and an embankment with a culvert (Fig. 1d). We also run an experiment (Experiment 1) using  
125 the bathtub approach, in which none of the above features are taken into account. These different setups can  
126 characterise different settings found in wetlands, but can also apply to different parts of a more complex wetland,  
127 as shown in Fig. 1b. In all ~~experiments~~ simulations the tidal flat is 620 m long (main flow direction) and 310 m  
128 wide (cross-section), divided into 10m by 10m grid cells, with a gentle slope of 0.001 m/m. Boundary conditions  
129 include input tides described by a sinusoidal function with 1.3 m amplitude and 12-hour period, and a constant  
130 sediment concentration at the wetland inlet (Fig. 1c). In each simulation~~experiment~~ we tested wetland evolution  
131 under sea-level rise from 2000 to 2100 (high emissions scenario) considering two sediment input conditions, a  
132 low sediment supply representing current conditions and a high sediment supply. The high sediment supply  
133 condition simulations are justified due to the uncertainty of climatic conditions and the possibility of increases in  
134 intensity of storm patterns in the area, which may result on increased sediment loads in the Hunter River. Sediment  
135 loads may also increase due to changes in land use practices (Rodriguez et al., 2020).

136 The sinusoidal tide represents conditions typical of SE Australian estuaries (Rodriguez et al., 2017) and is repeated  
137 during the simulation period (100 years). However, the mean water level is gradually increased following the  
138 IPCC RCP 8.5 scenario of sea-level rise (Church et al., 2013) with an expected 0.74 m increase by year 2100 with  
139 respect to the levels in the year 2000.

140 We use as a basis for our simulations the ecogeomorphological model (EGM) framework developed by Rodriguez  
141 et al. (2017), but with the addition of a physically-based sediment transport formulation. This EGM framework  
142 has been extensively calibrated and tested in the Hunter River Estuary in Australia and, as such, vegetation  
143 functions and parameters correspond to local conditions. The framework couples multiple models to simulate  
144 interactions between overland flow hydrodynamics, vegetation establishment and growth, sediment concentration  
145 and morphodynamics of the wetland.

## 146 **2.2 Hydrodynamic model**

147 Water depth time series over the tidal flat are estimated using a finite-differences quasi-2D hydrodynamic model  
148 (Riccardi, 2000) that has been successfully applied to coastal wetlands (Rodriguez et al., 2017;Sandi et al., 2018)  
149 and floodplains (Sandi et al., 2019;Sandi et al., 2020a;Sandi et al., 2020b;Saco et al., 2019). The model solves the  
150 shallow water equations using a cells scheme, in which cells are classified into tidal flat or channel categories to  
151 speed up computations. As previously explained, the domains of all simulation~~experiments~~ are 630 m long by  
152 310 m wide, discretised into 10mx10m cells. For cells representing channels in simulations 3 and 5, the width of  
153 the cell is reduced to 5 m and the elevation is lowered by 0.4 m. Boundary conditions include water elevations at  
154 the tidal creek and no-flow at the lateral and landward boundaries. Because the domains are wide, the effects of  
155 lateral model boundaries are minimal.

156 In each timestep, the model solves for water elevations at every cell using mass conservation in a 2D formulation,  
 157 and then it solves for discharges between cells in each direction using momentum conservation in a 1D  
 158 formulation. ~~The model solves for water elevations at cells and discharges between cells at each time step.~~ Mass  
 159 conservation is solved first to compute water surface elevations:

$$160 \quad As_i \frac{dz_i}{dt} = \sum_{k=1}^j Q_{k,i},$$

$$161 \quad (1)$$

162 where  $As_i$  and  $z_i$  are surface wetted area and water surface elevation at cell  $i$ , respectively and  $Q_{k,i}$  are the  
 163 discharges between cell  $i$  and its  $j$  neighbouring cells. Using the water surface elevations, the model then computes  
 164 discharges between cells using the momentum or energy equation, depending on the particular characteristics of  
 165 the connection between cells. For instance, the discharge between two cells on the vegetated tidal flat is computed  
 166 as:

$$167 \quad Q_{k,i} = \frac{A_{k,i} R_{k,i}^{\frac{2}{3}}}{n_{k,i}} \left( \frac{z_k - z_i}{x_k - x_i} \right)^{\frac{1}{2}},$$

$$168 \quad (2)$$

169 where  $A_{k,i}$ ,  $R_{k,i}$  and  $n_{k,i}$  are respectively the cross-sectional values of area, wetted perimeter and Manning  
 170 roughness computed as an average of the values at cells  $k$  and  $i$ , and  $x_k - x_i$  is the distance between cells. Based  
 171 on Rodriguez et al. (2017) we adopt roughness coefficients for mangrove and saltmarsh cells of  $0.50 \text{ s/m}^{1/3}$  and  
 172  $0.15 \text{ s/m}^{1/3}$ , respectively. For freshwater and no-vegetated cells, the Manning's- $n$  is  $0.12 \text{ s/m}^{1/3}$ , while for channel  
 173 cell it is  $0.035 \text{ s/m}^{1/3}$ . For cells in the channel, the full momentum equation is used to account for dynamic and  
 174 backwater effects (Riccardi, 2000). If the domain includes a culvert at cell  $i$ , then the discharge between cells  $k$   
 175 and  $i$  is computed as:

$$176 \quad Q_{k,i} = \frac{(2g)^{\frac{1}{2}} (z_k - z_i)^{\frac{1}{2}}}{\left( \frac{1}{C_d^2 A_i^2} - \frac{1}{A_k^2} \right)^{\frac{1}{2}}},$$

$$177 \quad (3)$$

178 in which  $A_i$  and  $A_k$  are respectively the cross-sectional areas at the  $i$  and  $k$  cells and  $C_d$  is a standard discharge  
 179 coefficient for the culvert at cell  $i$  adopted as 0.8. Equation (3) considered the case of the culvert flowing under  
 180 the influence of gravity. For pressurised conditions, a different equation is used (Riccardi, 2000)

181 The model equations are solved using an implicit method and a Newton-Raphson algorithm. The time step used  
 182 in the model solution is 1s to ensure numerical stability. Further explanation about the application of this model  
 183 in a similar EGM framework can be found in Sandi et al. (2018).

### 184 **2.3 Vegetation model**

185 Vegetation in coastal wetlands is driven by the tidal regime, so we use water depth time-series to compute the  
 186 mean depth below high tide,  $D$ , and the hydroperiod,  $H$ , on every cell as a descriptor of the tidal regime. These  
 187 variables are the input for all the other models of the EGM framework. The first variable represents the average  
 188 maximum water depth on spring tides. In this case we use a sinusoidal wave, so  $D$  is the maximum depth. The

189 hydroperiod accounts for the duration of the inundation period and is computed as the proportion of time during  
 190 which a minimum water depth is present during the simulation time.

191 The values of  $H$  and  $D$  define the suitable conditions for vegetation establishment and survival at each point in  
 192 the wetland based on thresholds that have been tested for SE Australian estuaries (Rodriguez et al., 2017). Thus,  
 193 the observed threshold applies to *Avicennia marina* (grey mangrove) and to a composition of saltmarsh species  
 194 *Sarcocornia quinqueflora* and *Sporobolus virginicus*. Mangrove depends primarily on hydroperiod, requires  
 195 frequent inundations and establishes in areas where  $10\% < H < 50\%$  and  $D > 0.2$  m, where  $H$  is calculated as the  
 196 fraction of time where the water depth is higher than or equal to 14 cm, the typical height of the pneumatophores.  
 197 Saltmarsh tolerates prolonged inundations and can survive in areas where  $H < 80\%$ , but cannot endure inundation  
 198 depths above its height (25 cm) so we limit  $D < 0.25$  m. We consider that, if conditions suit both mangrove and  
 199 saltmarsh, mangrove will expand over saltmarsh areas (Saintilan et al., 2014). In areas not exposed to saltwater  
 200 ( $H = 0\%$ ,  $D \sim 0$  m), we assume the presence of freshwater vegetation, and if none of the above conditions applies,  
 201 areas are considered to be non-vegetated.

## 202 2.4 Sediment model

203 The original version of the framework used in the Hunter estuary applies a linear empirical relationship between  
 204 average sediment concentration in the water column and the water depth. Here, we use a more physically based  
 205 equation for fine sediment transport and deposition processes coupled to the hydrodynamic simulations. The  
 206 sediment model solves the quasi-2D continuity equation of suspended sediment neglecting horizontal diffusion  
 207 (Garcia et al., 2015). The continuity equation for the  $i$ -th cell reads as follows:

$$208 \quad AS_i \frac{d(hC)_i}{dt} = AS_i \varphi_i + \sum_{k=1}^j (QC)_{k,i},$$

209 (4)

210 where  $h_i$  is the water depth of cell  $i$  (m);  $C_i$  is the sediment concentration ( $\text{g m}^{-3}$ ),  $\varphi_i$  is the downward vertical  
 211 flux of fine sediment ( $\text{g m}^{-2} \text{s}^{-1}$ ), and  $C_{k,i}$  are the sediment concentrations in the  $j$  neighbouring cells. For fine  
 212 grained sediment typical of estuarine environments, the downward flux can be expressed as (Krone, 1962; Mehta  
 213 and McAnally, 2008):

$$214 \quad \varphi_i = -w_s \left(1 - \frac{\tau_{bi}}{\tau_d}\right) C_i; \quad \tau_b < \tau_d,$$

215 (5)

216 where  $w_s$  is the fall/settling velocity of suspended sediment particles ( $\text{m s}^{-1}$ ),  $\tau_{bi}$  is the magnitude of bed shear  
 217 stress in cell  $i$  (Pa), and  $\tau_d$  is the critical ~~bed shear stress flow velocity~~ for deposition (Pa). Velocities where  
 218 converted to bed shear stresses using

$$219 \quad \tau_{bi} = \rho C_f U_i^2,$$

220 (6)

221 In equation (6)  $\rho$  is the water density and  $C_f$  is a friction coefficient set at 0.015. The parameters  $w_s$  and  $\tau_d$  were  
 222 varied to reproduce similar levels of accretion observed in the wetlands where the original modelling framework  
 223 was applied (Rodriguez et al., 2017). The values obtained were  $\tau_d = 0.01\text{--}02$  Pa and  $w_s = 2 \times 10^{-4}$  m/s, which are  
 224 consistent with values reported by Larsen et al. (2009) and Temmerman et al. (2005). This model does not have  
 225 an erosion term, which is not a bad simplification over vegetated surfaces that receive flows that are typically very  
 226 slow.

227 Equation (4) is solved using the same numerical scheme than the water mass conservation (equation 1) providing  
 228 a time series of sediment concentrations in each cell of the domain. However, as the soil elevation model (next  
 229 section) works at a larger time scale and requires the annual concentration,  $\bar{C}$ , a weighted average is computed for  
 230 each cell:

$$231 \quad \bar{C} = \frac{\sum_{t=0}^M (C_t \times h_t)}{\sum_{t=0}^M h_t},$$

232 (7)

233 where  $t$  is the time in the hydrodynamic simulation with  $M$  the final step,  $C_t$  and  $h_t$  are the sediment concentration  
 234 and the water depth, respectively, at time  $t$ .

235 The sediment transport equation based on mass conservation (eq. 4) cannot be used in the case of the bathtub  
 236 simulations because the bathtub model does not provide information on water discharge and velocity. For the  
 237 bathtub simulations, we used the linear relation between water depth and concentration empirically developed by  
 238 Rodriguez et al. (2017). Based on the measured data, the fitted equation is:

$$239 \quad \bar{C} = C_{max}(0.55D + 0.32),$$

240 (8)

241 where  $\bar{C}$  is the average sediment concentration ( $\text{g/m}^3$ ), and  $C_{max}$  is the concentration at the wetland inlet.

242 This equation is much simpler and has different parameters than the sediment transport equation; however, for  
 243 very simple flow conditions it should produce comparable results. We confirmed the suitability of the simple  
 244 model by comparing EGM results using the bathtub approach (with the linear sediment relation) and a full  
 245 hydrodynamic and sediment transport EGM over a smooth topography. Both the hydrodynamics and the resulting  
 246 elevation changes of both models were very similar (See [Figure-Fig. S1](#) in Supplementary Materials).

## 247 **2.5 Soil elevation change model**

248 Our EGM framework adopts the model originally proposed by Morris et al. (2002) and later modified by Kirwan  
 249 and Guntenspergen (2010) to estimate the increase in soil elevation due to accretion as function of hydrodynamic  
 250 and ecological conditions. We first compute the biomass production,  $B$  ( $\text{g/m}^2$ ), by using the parabolic equation:

$$251 \quad B = aD^2 + bD + c,$$

252 (9)

253 where  $a$ ,  $b$ , and  $c$  are parameters fitted to field data, for each vegetation type. Then, the surface elevation change  
 254 rate,  $dE/dt$  (m/year), is calculated using:

$$255 \quad \frac{dE}{dt} = \bar{C}(q + kB)D,$$

256 (10)

257 where  $q$  is a depositional parameter and  $k$  is a vegetation sediment trapping coefficient. For all five parameters of  
 258 equations (9) and (10) we used the values adopted in Rodriguez et al. (2017) and Sandi et al. (2018) (see Table 1)  
 259 for an Australian wetland. Although the term  $As_i \varphi_i$  in equation (4) provides an amount of settled sediment that  
 260 contributes to accretion, it only considers the gravitational settling of sediment and does not include many other  
 261 important accretion processes associated to the presence of vegetation. The full effects of sediment and vegetation  
 262 are considered in equation (10), which produces much larger accretion values (see Fig. S2 in Supplementary  
 263 Materials).

264 The EGM simulations use a yearly time-step, i.e. the computed biomass and accretion represent an average  
265 condition within this period. We choose a yearly time-step as vegetation dynamics does not respond  
266 instantaneously to flow and depositional processes (Alizad et al., 2016b; Saco and Rodríguez, 2013; Schuerch et  
267 al., 2018). Our model does not account for erosion and diffusion processes and also does not take into account the  
268 redistribution of deposited sediment by waves. Because of that, the resulting accretion from equation (10) is noisy  
269 and vary considerably over very short distances. In order to work with a more realistic distribution of deposition  
270 over the tidal flat we smooth the topography by applying a very simple diffusion model. The diffusion model does  
271 not change the general trends of deposition and avoids localised peaks of excessive deposition.

## 272 **3 Results**

### 273 **3.1 Spatial patterns of accretion and vegetation**

274 In order to show the characteristic spatial patterns of each of the typical cases analysed we first show in [Figure](#)  
275 [Fig. 2](#) accumulated accretion ( $\Delta E$ ) and vegetation distribution in 2050 under the expected SLR scenario for each  
276 of the five numerical [simulationexperiments](#), including the bathtub and the other four [simulationexperiments](#)  
277 that use a hydrodynamic and sediment transport (HST) models. Details on the temporal evolution of topography  
278 and vegetation for each of the [simulationexperiments](#) are provided later in the manuscript.

279 [Figure—Fig. 2](#) shows that accumulated accretion is homogeneous in the transverse direction for the  
280 [simulationexperiments](#) without the channel (Fig. 2a,b,d), as there is no lateral flow and the changes in  
281 sedimentation occur in the longitudinal direction only. For the [simulationexperiments](#) with the central drainage  
282 channel (Fig. 2 c,e) there is a marked concentration of flow and sediment accumulation close to the channel. Some  
283 of the accumulated accretion patterns of the [simulationexperiments](#) with the channel presented in [Figure—Fig. 2](#)  
284 are remarkably similar to the results from Chen et al. (2010) on a similar geometry.

285 It can be seen from the figure that all [simulationexperiments](#) show a general decrease of accretion with distance  
286 to the tidal input (which can represent a tidal creek or the river), which is expected because the source of sediment  
287 is at the tidal input. However, each [simulationexperiment](#) has a characteristic elevation profile and vegetation  
288 distribution, and they are all quite different from the predictions of the bathtub model. [Figure—Fig. 2a](#) shows that  
289 the bathtub [simulationexperiment](#) displays [a smoother and longer transition of accumulated accretion. A slight](#)  
290 [concentration of accretion is observed at 500 m from the creek, due to the initial position of high biomass](#)  
291 [saltmarsh](#)~~two depositional mounds, one at 300 m and the other at 500 m from the creek, which are due to the~~  
292 [initial position of high biomass areas of mangrove and saltmarsh, respectively, \(Figure 3a\) as it will be explained](#)  
293 [later](#). The bathtub case has flood and ebb flows of the same duration, since there is no flow attenuation. This keeps  
294 the hydroperiod within a range that promotes mangrove establishment over most of the wetland. Saltmarsh is  
295 limited to the upper parts of the tidal flat.

296 The other simulations ([Experiments-2 to 5](#)) use the hydrodynamic and sediment transport (HST) models instead  
297 of the bathtub approximation. In these cases, accretion presents an exponential shape with a sharper decrease than  
298 the bathtub model, and vegetation establishment is strongly controlled by the effects of vegetation roughness,  
299 channel and culverts. In contrast to the bathtub model results, all HST simulations show mangrove dieback in  
300 lower areas, which is caused by a higher hydroperiod due to attenuated ebb flows.



301 [ExperimentSimulation 2](#), with the undisturbed tidal flat ([Figure-Fig. 2b](#)), shows the effect of hydraulic resistance  
302 due to the vegetation roughness only, which generates an elevation mound closer to the tidal input than the bathtub  
303 [simulationexperiment](#). In [ExperimentSimulation 3](#) ([Figure-Fig. 2c](#)), the inner channel increases the drainage of  
304 the surrounding areas, thus reducing the hydroperiod in the vicinity of the channel and allowing mangroves to  
305 persist close to the tidal creek. The channel also enhances sediment delivery farther from the tidal input, which  
306 causes an increase in accretion around the mid-point of the flat (300 m from the tidal creek). However, this effect  
307 is concentrated near the channel and fades away as flow is directed into the tidal flat. In [ExperimentSimulation 4](#)  
308 ([Figure-Fig. 2d](#)), the flow is restricted by an embankment and a culvert, so the hydroperiods in the upper wetland  
309 are higher. This effect reduces mangrove migration and its encroachment on saltmarsh areas. In  
310 [ExperimentSimulation 5](#) with embankment and channel ([Fig. 2e](#)), the channel promotes mangrove landwards of  
311 the embankment, and also the stabilisation of saltmarsh areas in the upper sections of the tidal flat as they receive  
312 more sediment ([Figure-Fig. 2e](#)).

### 313 3.2 Evolution of accumulated accretion profiles

314 [Figure-Fig. 3](#) shows the results of surface elevation change ( $\Delta E$ ) in each [simulationexperiment](#) for the years 2020,  
315 2040, 2060 and 2100 for low sediment input conditions (corresponding to contemporary rates in the Hunter  
316 estuary), in terms of accumulated accretion profiles along the main flow direction. For the [simulationexperiments](#)  
317 with the central drainage channel ([SimulationsExperiments 3 and 5](#)), we have included two profiles at different  
318 transverse locations, one close to the channel and one 150 m away in the middle of the tidal flat.

319 During the first two decades, the vegetation type plays an important role in the longitudinal distribution of the  
320 accumulated accretion profiles. By 2020 (first column of [Figure 3](#)) the profiles show a continuous decrease from  
321 the tidal input up to 300 to 350 m approximately, which coincides with the transition from mangrove to saltmarsh  
322 in the initial vegetation distributions (see [Fig. 5](#) later in the manuscript). This occurs due to the dynamics of  
323 sediment transport (more deposition close to the tidal input) and also due to the reduction of the mangrove biomass  
324 away from the tidal creek (reductions in  $D$ , see eqn. 10). The increase in  $\Delta E$  at the transition is due to the saltmarsh  
325 having a higher biomass and trapping efficiency than mangrove at that particular value of  $D$ . Landward of the  
326 transition,  $\Delta E$  decreases with decreases in saltmarsh biomass. This general dynamics is disrupted by the presence  
327 of the culvert because it limits the amount of sediment reaching the upper areas of the tidal flat.

328 Changes in  $\Delta E$  slow down after 2060 in all [simulationexperiments](#) except for the bathtub case. This is due to  
329 reductions in vegetation as most of the lower areas of the tidal flat have experienced submergence and vegetation  
330 loss. Small increases in  $\Delta E$  occur in the upper areas in the cases in which the central channel promotes tidal  
331 flushing ([SimulationsExperiments 3 and 5](#)), but this effect is concentrated in areas close to the channel.

332 None of the [simulationexperiments](#) using the HST model produces  $\Delta E$  results similar to the bathtub simulations.  
333 The [simulationexperiment](#) with the central channel ([ExperimentSimulation 3](#)), presents values of  $\Delta E$  near the  
334 channel that are close to the results of the bathtub simulation during the first years, but over time, the results  
335 diverge. The increased  $\Delta E$  values are limited to areas next to the channel, and they quickly decline as the flow is  
336 directed into the tidal flat. In general, the outcomes from the HST model shows a reduction in the water levels and  
337 total accretion compared to the bathtub results. Furthermore, when the culvert is introduced in the simulation  
338 ([Experiments 4 and 5](#)), the main effect is a drastic reduction of  $\Delta E$  in the upper areas of the domain.

339 Fig.ure 3 results correspond to a situation with a low sediment input of 37 g/m<sup>3</sup>, typical of current SE Australia  
340 conditions (Rodriguez et al., 2017). Similar patterns but with larger values of accumulated accretion were obtained  
341 for a higher sediment input of 111 g/m<sup>3</sup> (Fig.ure S2-S3 in Supplementary Materials).

342 The reduction in accretion in the simulationexperiments that consider the actual features of the wetland can be  
343 better appreciated in Fig.ure 4, in which we compare domain-average  $\Delta E$  of all simulationexperiments over time.  
344 Fig.ure 4 includes results for a low sediment input of 37 g/m<sup>3</sup> (Fig.ure 4a) and for a high sediment input of 111  
345 g/m<sup>3</sup> (Fig.ure 4b). The figure also includes the values of mean sea-level for each year to give an idea of the  
346 submergence conditions in the wetlands.

347 There is a clear difference between the accretion generated in the bathtub simulation, and the rest of the  
348 simulationexperiments. In our simulations, accretion is a function of sediment concentration and depth below  
349 mean high tide ( $D$ ). The bathtub assumption overpredicts both inputs over the entire domain, thus generating  
350 higher accretion values. In all HST simulations, the combination of a reduction in  $D$  because of flow attenuation  
351 and the exponential decay of sediment concentration results in less accretion than in the bathtub  
352 simulationexperiment. In the case of low sediment input (Fig.ure 4a), by 2050 the domain-average  $\Delta E$  from the  
353 bathtub is about 2 times the values of all the other simulationexperiments, increasing to more than 3 times by  
354 2100. In the simulations with high sediment input (Fig.ure 4b), the accumulated accretion of bathtub simulations  
355 are 2.5 and 4 times the values of the rest of the simulationexperiments for 2050 and 2100, respectively. The  
356 simulationexperiments with the HST simulations present differentdifferent levels of attenuation and accordingly  
357 different accretion levels. The lowest accretion correspond to the highly attenuated case with embankment and  
358 culvert (Exp.Sim. 4), whereas the highest accretion occur in the case of the central channel (Exp.Sim. 3) that  
359 experiences increased drainage and thus less attenuation. The cases of the tidal flat with no structures (Exp.Sim.  
360 2) and of the embankment with inner channel (Exp.Sim.5) have intermediate levels of attenuation and accretion.  
361 All simulations show a strong elevation deficit (i.e. the difference between the rate of sea level rise and wetland  
362 accretion rate  $dE/dt$ ), as none of the simulationexperiments predict that the tidal flat is capable to keep pace with  
363 SLR. For the low-sediment conditions, by 2050 the elevation deficit of the bathtub simulation is 5.5 mm/yr, while  
364 the rest of the simulationexperiments predict an elevation deficit of about 7 mm/yr. Over time, the elevation  
365 deficits increase and by 2100 the bathtub prediction reach a value of 9.5 mm/yr and the HST simulations a value  
366 of 12 mm/yr.

367 Increasing the sediment input concentration considerably changes the accretion capacity of the tidal flat,  
368 particularly according to the bathtub results. Bathtub simulations predict that the tidal flat is able to accrete in a  
369 rate that almost match the changes in sea level, so the wetland survives sea-level rise. Accretion for all other  
370 simulationexperiments are moderate, with the simulationexperiments that have the central channel (Experiments  
371 3 and 5) responding more effectively to the increased sediment and accreting more than the other  
372 simulationexperiments (Exp.Sim. 2 and 4). Compared to the low sediment conditions, elevation deficits of the  
373 bathtub predictions reduce to 3 mm/yr and 5.5 mm/yr by 2050 and 2100, respectively, while in the other  
374 simulationexperiments those values increase to about 6 mm/yr and 10 mm/yr.

375 The structures included in the simulations have a clear effect on the average  $\Delta E$ . The inner channel promotes  
376 accretion further inland, as it conveys more water and sediment to those areas away from the tidal input. Compared  
377 to the tidal flat free of structures (ExperimentSimulation 2) the inclusion of the channel (ExperimentSimulation  
378 3) is responsible for an increase in wetland accumulated accretion of about 50%. The opposite effect is observed

379 when the embankment with culvert is introduced, as it attenuates and reduces the water and sediment flow into  
380 the upper part of the wetland. Comparing results for the tidal flat without ([ExperimentSimulation 2](#)) and with  
381 ([ExperimentSimulation 4](#)) embankment and culvert, we can observe a reduction on wetland accumulated accretion  
382 of 25%. The introduction of a drainage channel together with the embankment and culvert ([ExperimentSimulation](#)  
383 5) represents an intermediate situation in which the increased flushing effect of the channel and the attenuating  
384 effect of the embankment and culvert partially compensate.

385 In [Figure 4a](#) we have also included the average accumulated accretion for the entire wetland site (Area E in [Figure](#)  
386 [Fig. 1b](#)) using information from Rodriguez et al. (2017) and (Sandi et al., 2018). Rodriguez et al. (2017) applied  
387 a similar EGM formulation to Area E ([Fig. 1c](#)) to assess the effect of attenuation on wetland evolution under SLR  
388 considering typical ( $37 \text{ mg/m}^3$ ) and increased ( $111 \text{ mg/m}^3$ ) sediment conditions. (Sandi et al., 2018) further studied  
389 the effects of tidal restrictions at the wetland inlet considering typical sediment loads. The values included in the  
390 figure correspond to average accumulated accretion over the entire wetland at 2050 and 2100 for low sediment  
391 load with and without tidal restrictions ([Figure-Fig. 4a](#)) and for high sediment load without restrictions ([Figure](#)  
392 [Fig. 4b](#)). The figures shows that the simulations without tidal ~~restrieions~~restrictions result in values of accumulated  
393 accretion similar to the [simulationexperiment](#) with low attenuation ([Experiments-Simulations 3 and 5](#)) for both  
394 low and high sediment loads, while predictions of accumulated accretion including tidal restrictions are closer to  
395 the [simulationexperiment](#) with high attenuation ([SimulationExperiments 2 and 4](#)).

### 396 3.3 Changes in vegetation

397 The interactions between sea-level rise, accretion and vegetation changes are complex because vegetation not  
398 only responds to vertical elevation changes but also migrates inland. In order to obtain a clear picture of the  
399 vegetation changes over time, we simplified two dimensional vegetation maps (i.e., [Figure 2](#)) into a one-  
400 dimensional representation. The vegetation type at a given distance from the tidal input was determined by  
401 selecting the predominant (higher occurrence) vegetation in the transverse direction. [Fig. 5](#) shows snapshots of  
402 the predominant vegetation every 20 years. As already explained, in the simulations with embankment and culvert  
403 ([Simulations 4 and 5](#)), the structures are located at 310 m from the tidal input. The conditions at the beginning of  
404 the simulation ([Fig. 5a](#)) for [simulationexperiments 1, 2, and 3](#) show mangrove occupying approximately the  
405 lower 400 m of the tidal flat and saltmarsh the next 200 m upland. For [simulationexperiments 4 and 5](#) the presence  
406 of the embankment reduces hydroperiods in the upper areas, constraining mangrove to the lower 310 m. The  
407 embankment also limits the extent of inundation in the upper areas, reducing the extent of the saltmarsh to about  
408 100 m from the embankment.

409 After 20 years ([Figure 5b](#)) the [simulations 1, 2 and 3simulations](#) show mangrove encroachment on saltmarsh  
410 [experiments 1, 2 and 3](#). The upstream mangrove edge moves up to 50 m, forcing saltmarsh occurrence in areas  
411 further than 300 m from the tide input creek. In [simulationexperiments 4 and 5](#) the embankment halts mangrove  
412 migration and increases in inundation of upper areas promote saltmarsh increase. Overall, wetland area increases  
413 due to mangrove expansion ([ExpSim. 1, 2 and 3](#)) or to saltmarsh expansion ([ExpSim. 4 and 5](#)).

414 By 2040 ([Figure-Fig. 5c](#)), mangrove has encroached further on saltmarsh in [simulationexperiments 1, 2 and 3](#),  
415 resulting in saltmarsh squeeze at the upper end due to the landward boundary of the computational domain.  
416 [Experiments-Simulations 4 and 5](#) show very minor encroachment of mangrove on saltmarsh, which is able to  
417 migrate landward. Total wetland area remains approximately unchanged for [simulationexperiments 1, 2 and 3](#),

418 while it keeps increasing in simulationexperiments 4 and 5. Some areas of mudflat start appearing in the HST  
419 simulationexperiments due to extended hydroperiods.

420 Twenty years later, in 2060 (Figure 5d), the MSL is about 30 cm higher than in 2000 and we can see considerable  
421 mudflat areas in all experiments-simulations except for the bathtub simulation (Simulationexperiment 1), which  
422 presentspresents a uniform coverage of mangrove over the entire domain. Saltmarsh is totally absent in experiments  
423 simulations 1, 2 and 3 due to mangrove encroachment but still remains almost unchanged in experiments  
424 simulations 4 and 5. All simulationexperiments except the bathtub simulation show decreases in wetland extent,  
425 mostly due to saltmarsh dissaparaneedisappearance in experiments-simulations 2 and 3 and to mangrove squeeze  
426 in simulationexperiments 4 and 5.

427 From 2080 on (Figures-Fig. 5e,f), a rapid retreat of the remaining wetland can be observed in all  
428 simulationexperiments. The retreat occurs faster for the simulationexperiments with the embankment, resulting  
429 in total wetland disappearance by 2100. The rest of the simulationexperiments still show some remnant mangrove  
430 areas by 2100, which are only significant (40%) in the case of the bathtub simulations.

431 The same trend of increase in wetland area in the first 20 years of simulation, followed by a continuous decrease  
432 starting at 40 years and ending at 100 years with almost complete wetland disappearance under the same sea level  
433 rise trajectory was observed by Rodriguez et al. (2017) and Sandi et al. (2018). Sandi et al. (2018) also reported  
434 larger wetland losses for-in their simulationexperiments with tidal input restrictions at the entrance-wetland inlet  
435 when compared to the case without restrictions.

436 The same analysis of vegetation evolution for the high sediment input scenario is presented in Figure 6. With  
437 increased sediment, the patterns of vegetation change remain remarkably similar to the patterns observed in Figure  
438 Fig. 5 for the low sediment conditions, with exception of the bathtub simulations (ExperimentSimulation 1).  
439 Compared to Figure-Fig. 5, the bathtub results indicate that saltmarsh is able to remain in the upper wetland areas  
440 for longer (until 2060) and that mangrove does not retreat, resulting in no wetland loss after 100 years of  
441 simulation. The other simulationexperiments without embankment (2 and 3) show a slightly slower retreat of  
442 both mangrove and saltmarsh than in Figure-Fig. 5, while the simulationexperiments with the embankment show  
443 almost the same behaviour as the in the case of low sediment. Some of simulationexperiments in Figure 6 show  
444 localised mangrove areas that tend to establish and persist close to the tidal creek.

445 For a more detailed analysis we can look at the vegetation evolution in terms of wetland area (mangrove and  
446 saltmarsh), wetland retreat (position of the seaward edge) and wetland transgression (position of the landward  
447 edge).

448 Fig. 7a shows that the wetland extent predicted using the bathtub approach (Simulation 1) is affected by the  
449 sediment load, with only the low sediment condition resulting in a sharp decay in extent after 2060/70. The  
450 difference in extent is due to the vegetation retreat in the low sediment case, which does not occur in the high  
451 sediment case (Fig. 7b). Wetland extent values for the HST simulations are not greatly affected by the sediment  
452 load, and they are much smaller than the values predicted by the bathtub (Fig. 7a). Wetland retreat starts first in  
453 the simulations without the channel (Simulations. 2 and 4) and about 20 years later in the simulations with the  
454 channel (Simulations 3 and 5) due to increased drainage. Once the retreat starts, it occurs faster in the simulations  
455 with the embankment (Simulations 4 and 5) that delays the ebb flows and increases hydroperiods in the lower  
456 wetland areas.

457 Wetland transgression is not affected by the sediment conditions (Fig. 7c) because of the limited amount of  
458 sediment that reaches the upper wetland areas. Transgression starts later in the simulations with the embankment  
459 (Simulations 4 and 5) because of the reduced depths and sediment loads in the upper wetland areas. The presence  
460 of the channel (Simulations 3 and 5) results in earlier but more gradual transgression compared to setups with no  
461 drainage structure (Simulations 2 and 4).

#### 462 **4 Discussion**

463 The interactions between all the processes related to the dynamic of coastal wetlands are quite complex  
464 (Fagherazzi et al., 2012; Reef et al., 2018; Saintilan et al., 2014), which makes the bathtub assumption limited for  
465 most applications. Places with multiple vegetation species (Cahoon et al., 2011; Rogers et al., 2006) and an  
466 intertwined channel network (D'Alpaos, 2011) present a strong heterogeneity of saltwater exposure and sediment  
467 delivery to the overbank areas that need a detailed description of flow and sediment processes (see also Coleman  
468 et al., 2020). Artificial structures constraining flow and sediment modify accretion rates (Bellafiore et al.,  
469 2014; Cahoon et al., 2011) and thus wetland evolution (Rodriguez et al., 2017; Sandi et al., 2018). Even though our  
470 experimental-simulation design focused on simplified setups, these setups comprise typical wetland features and  
471 include most of the complex processes and interactions.

472 Our results indicate that wetlands do not cope with SLR for the simulated conditions corresponding to a high  
473 emissions climate change scenario. This result was not surprising for the low sediment situation, as the inability  
474 of sediment-poor coastal wetlands to survive high levels of SLR due to low accretion rates has been reported  
475 before (Kirwan et al., 2010; Lovelock et al., 2015b; Rodriguez et al., 2017; Sandi et al., 2018; Schuerch et al., 2018).  
476 However, the results for high sediment load seem to challenge some previous studies highlighting the potential of  
477 biophysical feedbacks to produce accretion rates comparable to SLR (D'Alpaos et al., 2007; Kirwan  
478 and Murray, 2007; Kirwan et al., 2016b; Mudd et al., 2009; Temmerman et al., 2003). In our case, the biophysical  
479 feedbacks with a high sediment load produced wetland accretion rates similar to SLR rates only for the bathtub  
480 simulation.

481 Analysis of accretion rates indicate that all simulation-experiments start with similar rates in the vegetated areas,  
482 with about 2.5 mm/yr and 7.5 mm/yr in the low and high sediment situation, respectively. For the low sediment  
483 case, the initial value compared very well with historic values for SE Australian -conditions measured by Howe  
484 et al. (2009) and Rogers et al. (2006). For the high sediment case, an increase of the accretion value by a factor of  
485 three seems reasonable considering an increase of the sediment load by a factor of three (from 37 g/m<sup>3</sup> to 111  
486 g/m<sup>3</sup>). Those starting values of accretion remain at approximately the same level over most of the time for the  
487 bathtub simulations, while they decrease for the HST simulations. The decrease is more marked for  
488 Exps-Simulations 2 and 4 (which reach a value of about 1 to 1.5 mm/yr by 2050), than for the simulations with  
489 inner channel Exps-Simulations 3 and 5 (which attain values of 2 mm/yr and 4 mm/yr by 2050 for low and high  
490 sediment conditions, respectively). The reduction of the magnitude of the biophysical feedbacks over time is due  
491 to the continuous upland migration of vegetation, which colonises upper areas with comparatively less water depth  
492 and sediment supply (see also Sandi et al. (2018)). The bathtub model predicts less migration and higher depths,  
493 so it consistently overestimates accretion rates.

494 Despite having reduced accretion rates when compared to the bathtub simulations, the HST simulations still show  
495 a noticeable difference in elevation gains depending on the sediment supply levels. Compared to the low sediment

496 case, the high sediment supply case results in about twice the average accumulated accretion (Fig.ure 4). However,  
497 analysis of vegetation changes over time for low (Fig.ure 5) and high (Fig.ure 6) sediment loads reveal minimum  
498 differences between them. ~~For a more detailed analysis we can look at the vegetation evolution in terms of wetland~~  
499 ~~area (mangrove and saltmarsh), wetland retreat (position of the seaward edge) and wetland transgression (position~~  
500 ~~of the landward edge), as presented in Figure 7.~~  
501 ~~Figure 7a shows that the wetland extent predicted using the bathtub approach (Exp. 1) is affected by the sediment~~  
502 ~~load, with only the low sediment condition resulting in a sharp decay in extent after 2060/70. The difference in~~  
503 ~~extent is due to the vegetation retreat in the low sediment case, which does not occur in the high sediment case~~  
504 ~~(Figure 7b). Wetland extent values for the HST simulations are not greatly affected by the sediment load, and they~~  
505 ~~are much smaller than the values predicted by the bathtub (Figure 7a). Wetland retreat starts first in the~~  
506 ~~experiments without the channel (Exps. 2 and 4) and about 20 years later in the experiments with the channel~~  
507 ~~(Exps. 3 and 5) due to increased drainage. Once the retreat starts, it occurs faster in the experiments with the~~  
508 ~~embankment (Exps. 4 and 5) that delays the ebb flows and increases hydroperiods in the lower wetland areas.~~  
509 ~~Wetland transgression is not affected by the sediment conditions (Figure 7c) because of the limited amount of~~  
510 ~~sediment that reaches the upper wetland areas. Transgression starts later in the experiments with the embankment~~  
511 ~~(Exps. 4 and 5) because of the reduced depths and sediment loads in the upper wetland areas. The presence of the~~  
512 ~~channel (Exp. 3 and 5) results in earlier but more gradual transgression compared to setups with no drainage~~  
513 ~~structure (Exp. 2 and 4).~~  
514 ~~It is clear from the a~~ analysis of Fig.ure 7 indicates that even though the increase in sediment load generates about  
515 twice the accretion, this extra elevation is not sufficient to prevent wetland submergence. Fig.ure 4 suggests that  
516 accretion rates of four times the historic values or more are needed for the wetlands to be able to cope with SLR.  
517 Although the simulations carried out in this study were conducted on simplified domains they can capture the  
518 general response of more complex domains present in real wetlands, as shown by the comparison with entire  
519 wetland results from Rodriguez et al. (2017) and Sandi et al. (2018) in Figure 4. Moreover, the features included  
520 are present in many coastal areas around the world and thus have wider ,~~the features included are present in many~~  
521 ~~coastal areas around the world an thus have wider implications. Our~~ implications. Our bathtub results for low  
522 sediment conditions predicting an initial increase in wetland extent early in the century and then a decrease after  
523 2060 agree with previous bathtub model predictions (Lovelock et al., 2015b;Rogers et al., 2012;Schuerch et al.,  
524 2018). However, using the HST framework our predictions indicate that the decrease may start as early as 2030  
525 for wetlands with tidal range close to 1.3 m (as represented in our study), over a wide range of sediment loads.  
526 We can expect that this accelerated wetland loss will affect many parts of the world, particularly in areas with  
527 micro to meso tidal range and heavily developed coasts, like eastern Australia (Williams and Watford, 1997),  
528 parts of eastern US (Crain et al., 2009), western US (Thorne et al., 2018) eastern China (Tian et al., 2016) and  
529 western Europe (Gibson et al., 2007). In these environments, attenuation can be important due to man-made  
530 structures, and transgression may be limited by development (Doody, 2013;Geselbracht et al., 2015;Kirwan and  
531 Megonigal, 2013), so we can expect a behaviour closer to that of simulationexperiments 4 and 5. On the other  
532 hand, wetlands with dense drainage networks like the Venice Lagoon in Italy (Silvestri et al., 2005), the Scheldt  
533 Estuary in the Netherlands (Temmerman et al., 2012), the North Inlet in South Carolina, US (Morris et al., 2005),  
534 would probably behave similarly to simulationexperiment 3 and experience comparatively less-smaller losses of  
535 area.

536 The results presented in this study show generalized conditions of wetland dynamics under sea-level rise by using  
537 several simplified domains that focus on individual mechanisms affecting ecogeomorphic evolution. This  
538 approach can support a broader perspective on the potential fate of coastal wetlands in general, but some  
539 limitations arise as part of the model assumptions. As with most wetland evolution models, we did not consider  
540 soil processes other than accretion, disregarding swelling, compaction and deep subsidence. Measurements in  
541 wetlands of the Hunter Estuary show that long-term surface elevation changes are mostly due to accretion,  
542 supporting our assumption (Howe et al., 2009; Rogers et al., 2006). Another process that we did not consider was  
543 the effects of marsh edge retreat due to ocean or wind waves (Carniello et al., 2012; Fagherazzi et al., 2012), which  
544 can have a significant role in coastal wetland evolution. Most coastal wetlands in Australia are estuarine and not  
545 exposed to ocean waves, whereas wind effects in our wetland were not important due to the absence of large open  
546 water areas where wind waves could fully develop. We also simplified the tidal signal without including neap-  
547 spring cycles, which sped up computations but may have affected the results. However, preliminary tests including  
548 neap-spring tide variability showed only small differences in the initial landward edge of saltmarsh, which did not  
549 affect the accretion dynamics due to the small depths and low sediment availability in that area. Finally, our  
550 simulations did not include the effect of storms, which can influence sediment availability, water depths and  
551 velocities. We believe that in our case excluding storm effects is justifiable based on Rogers et al. (2013), who  
552 found that in these fine sediment environments storms affect accretion dynamics over the short term (immediate  
553 erosion or low accretion followed by increased deposition over the next months), but they do not change the long-  
554 term trend of accretion and elevation gain rates.

## 555 **5 Conclusion**

556 We conducted detailed numerical simulationexperiments on the response to SLR of four different typical coastal  
557 wetlands settings, including the case of a vegetated tidal flat free from obstructions and drainage features, and  
558 three other settings that included an inner channel, an embankment with a culvert, and a combination of inner  
559 channel, embankment and culvert. We also included an simulationexperiment using a simple bathtub approach,  
560 in which none of the features (vegetation, channels, culverts) are considered. We used conditions typical of SE  
561 Australia in terms of vegetation, tidal range and sediment load, but we also analysed simulations with an increased  
562 sediment load to assess the potential of biophysical feedbacks to enhance accretion rates.

563 We found that the distinct patterns of flow and sediment redistribution obtained from these simulations result in  
564 increased wetland vulnerability to SLR when compared to predictions using the simple bathtub approach. Changes  
565 in elevation due to accretion were between 10% and 50% of those obtained from bathtub predictions, and wetland  
566 retreat and reduction of wetland extent started 20 to 40 years earlier than for the case of the bathtub simulations,  
567 depending on wetland setting. Transgression for all settings was delayed with respect to the bathtub predictions  
568 and was limited by the presence of a hard barrier at the upland end.

569 The simulations using the full hydrodynamic and sediment transport dynamic models indicated that wetlands with  
570 good drainage (e.g. including an inner channel) were more resilient to SLR, displaying more accretion, a later  
571 retreat and reduction of wetland area and an increased transgression when compared with wetlands with strong  
572 flow impediments (e.g. including an embankment).

573 IneresingIncreasing the sediment load delivered to the wetlands by a factor of three increased the accretion of all  
574 wetland settings by a factor of two. However, this extra elevation was not enough to prevent wetland submergence,

575 as predictions of wetland evolution were very similar for low and high sediment conditions. Based on our results,  
576 we estimate that accretion rates of four times the typical historic values or more would be needed for these  
577 wetlands to cope with SLR.

578 Even though the characteristics of the wetlands studied here correspond mainly to SE Australian conditions, our  
579 results have a wider relevance because they clearly link the capacity of wetlands to accrete and migrate upland,  
580 the two mechanisms by which wetlands can gain elevation and keep up with SLR. Failure to consider the spatial  
581 coevolving nature of flow, sediment, vegetation and topographic features can result in overestimation of wetland  
582 resilience. Our results reconcile the wide discrepancy between upper thresholds of wetland resilience to sea-level  
583 rise in previous modelling studies with those emerging from [palaeopalco](#)-stratigraphic observations.

584

585 *Data availability.* Upon acceptance of the manuscript, the hydrodynamic model and simulation results will be  
586 available from the corresponding authors on request.

587

588 *Competing interests.* The authors declare that they have no conflict of interest.

589

590 *Author contribution.* A.B., P.M.S. and J.F.R. designed the study. A.B. calibrated and fitted the models and run the  
591 simulations. A.B., J.F.R., P.M.S., S.S., G.R. and N.S. analysed the results. A.B., P.M.S. and J.F.R. wrote the paper  
592 with substantial input from all co-authors.

593

594 *Acknowledgements.* P.M.S. acknowledges support from the Australian Research Council (grant FT140100610).  
595 A.B. was supported by a University of Newcastle PhD scholarship.

## 596 **References**

- 597 [1] Alizad, K., Hagen, S. C., Morris, J. T., Bacopoulos, P., Bilskie, M. V., Weishampel, J. F., and Medeiros,  
598 S. C.: A coupled, two-dimensional hydrodynamic-marsh model with biological feedback, *Ecol Model*,  
599 327, 29-43, 10.1016/j.ecolmodel.2016.01.013, 2016a.
- 600 [2] Alizad, K., Hagen, S. C., Morris, J. T., Medeiros, S. C., Bilskie, M. V., and Weishampel, J. F.: Coastal  
601 wetland response to sea-level rise in a fluvial estuarine system, *Earths Future*, 4, 483-497,  
602 10.1002/2016ef000385, 2016b.
- 603 [3] Bellafiore, D., Ghezzi, M., Tagliapietra, D., and Umgiesser, G.: Climate change and artificial barrier  
604 effects on the Venice Lagoon: Inundation dynamics of salt marshes and implications for halophytes  
605 distribution, *Ocean Coast Manage*, 100, 101-115, 10.1016/j.ocecoaman.2014.08.002, 2014.
- 606 [4] Belliard, J. P., Di Marco, N., Carniello, L., and Toffolon, M.: Sediment and vegetation spatial dynamics  
607 facing sea-level rise in microtidal salt marshes: Insights from an ecogeomorphic model, *Adv Water*  
608 *Resour*, 93, 249-264, 10.1016/j.advwatres.2015.11.020, 2016.
- 609 [5] Beudin, A., Kalra, T. S., Ganju, N. K., and Warner, J. C.: Development of a coupled wave-flow-  
610 vegetation interaction model, *Computers & Geosciences*, 100, 76-86,  
611 <https://doi.org/10.1016/j.cageo.2016.12.010>, 2017.
- 612 [6] Bilskie, M. V., Hagen, S. C., Alizad, K., Medeiros, S. C., Passeri, D. L., Needham, H. F., and Cox, A.:  
613 Dynamic simulation and numerical analysis of hurricane storm surge under sea level rise with  
614 geomorphologic changes along the northern Gulf of Mexico, *Earths Future*, 4, 177-193,  
615 10.1002/2015ef000347, 2016.
- 616 [7] Cahoon, D. R., Perez, B. C., Segura, B. D., and Lynch, J. C.: Elevation trends and shrink-swell response  
617 of wetland soils to flooding and drying, *Estuar Coast Shelf S*, 91, 463-474, 10.1016/j.ecss.2010.03.022,  
618 2011.

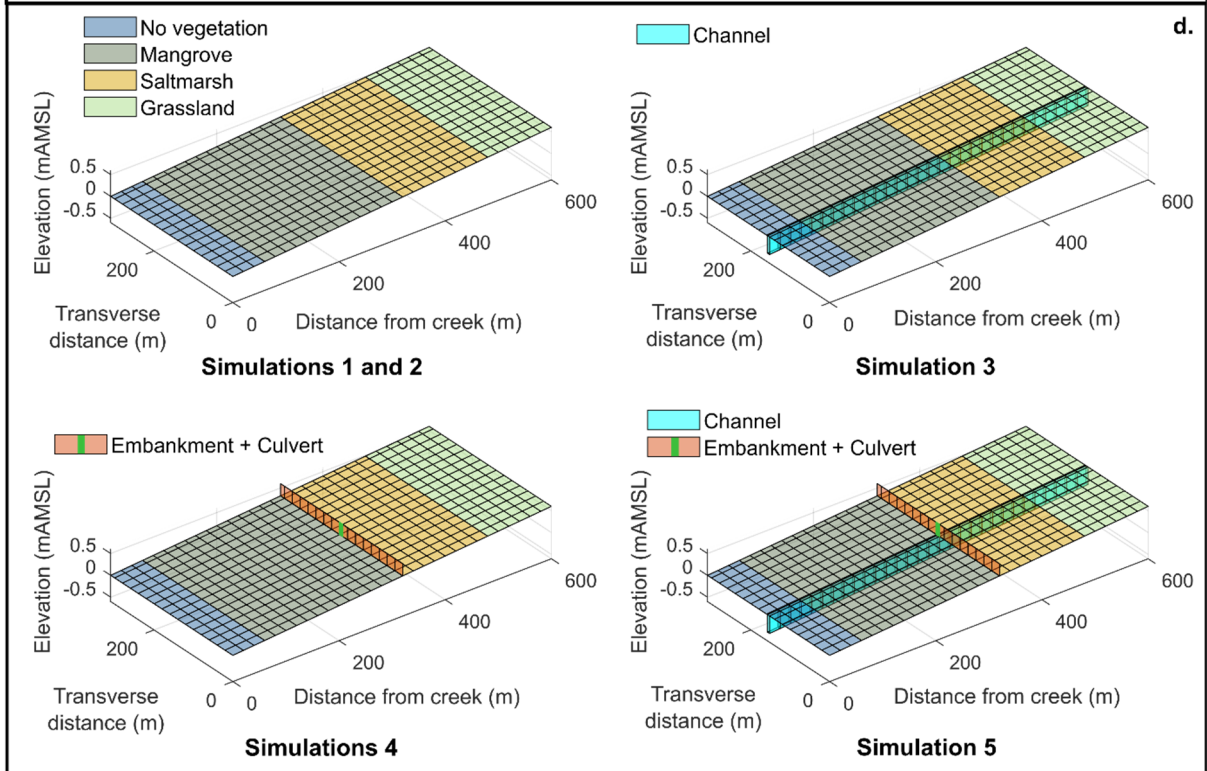
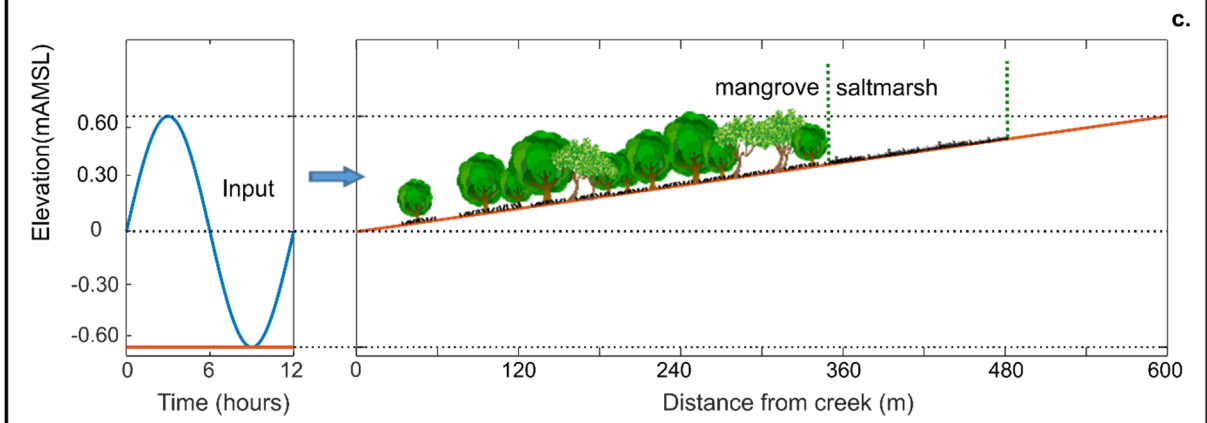
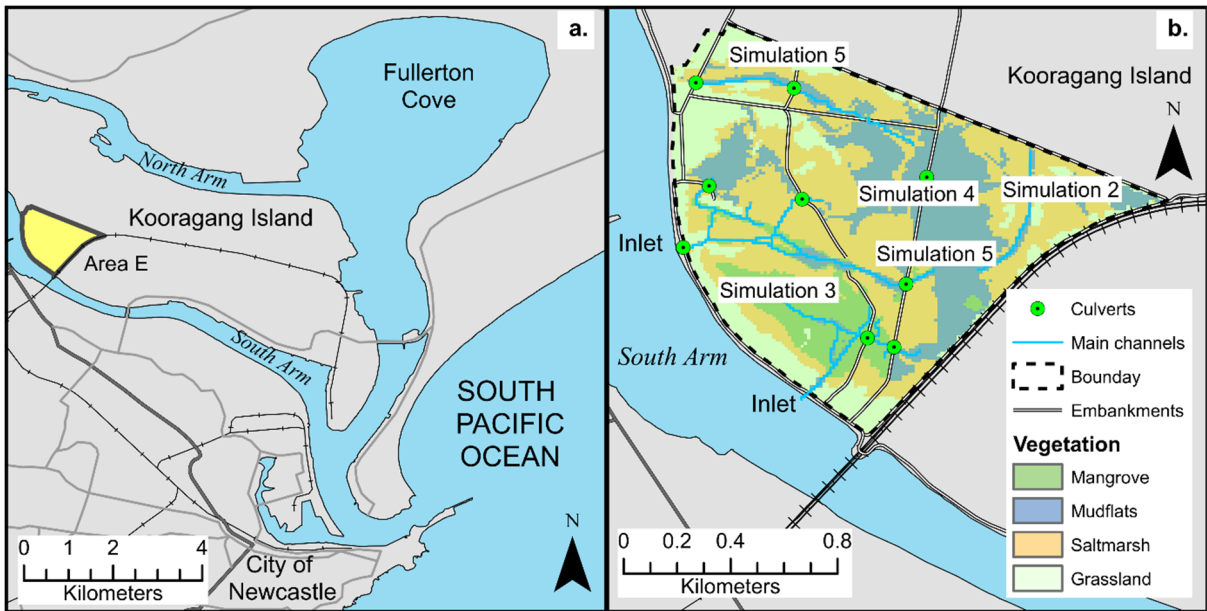


- 619 [8] Carniello, L., Defina, A., and D'Alpaos, L.: Modeling sand-mud transport induced by tidal currents and  
620 wind waves in shallow microtidal basins: Application to the Venice Lagoon (Italy), *Estuar Coast Shelf*  
621 *S*, 102, 105-115, 10.1016/j.ecss.2012.03.016, 2012.
- 622 [9] Chen, S. N., Geyer, W. R., Sherwood, C. R., and Ralston, D. K.: Sediment transport and deposition on a  
623 river-dominated tidal flat: An idealized model study, *J Geophys Res-Oceans*, 115, Artn C10040,  
624 10.1029/2010jc006248, 2010.
- 625 [10] Church, J. A., Clark, P. U., Cazenave, A., Gregory, J. M., Jevrejeva, S., Levermann, A., Merrifield, M.  
626 A., Milne, G. A., Nerem, R. S., Nunn, P. D., Payne, A. J., Pfeffer, W. T., Stammer, D., and Unnikrishnan,  
627 A. S.: Sea Level Change, in: *Climate Change 2013: The Physical Science Basis. Contribution of Working*  
628 *Group I to the Fifth Assessment Report of the Intergovernmental Panel on Climate Change*, edited by:  
629 Stocker, T. F., Qin, D., Plattner, G.-K., Tignor, M., Allen, S. K., Boschung, J., Nauels, A., Xia, Y., Bex,  
630 V., and Midgley, P. M., Cambridge University Press, Cambridge, UK and New York, USA, 1137-1216,  
631 2013.
- 632 [11] Clough, J., Polaczyk, A., and Propato, M.: Modeling the potential effects of sea-level rise on the coast  
633 of New York: Integrating mechanistic accretion and stochastic uncertainty, *Environ Modell Softw*, 84,  
634 349-362, 10.1016/j.envsoft.2016.06.023, 2016.
- 635 [12] Crain, C. M., Halpern, B. S., Beck, M. W., and Kappel, C. V.: Understanding and Managing Human  
636 Threats to the Coastal Marine Environment, *Year in Ecology and Conservation Biology 2009*, 1162, 39-  
637 62, 10.1111/j.1749-6632.2009.04496.x, 2009.
- 638 [13] Crase, B., Liedloff, A., Vesik, P. A., Burgman, M. A., and Wintle, B. A.: Hydroperiod is the main driver  
639 of the spatial pattern of dominance in mangrove communities, *Global Ecol Biogeogr*, 22, 806-817,  
640 10.1111/geb.12063, 2013.
- 641 [14] D'Alpaos, A., Lanzoni, S., Marani, M., and Rinaldo, A.: Landscape evolution in tidal embayments:  
642 Modeling the interplay of erosion, sedimentation, and vegetation dynamics, *J Geophys Res-Earth*, 112,  
643 Artn F01008, 10.1029/2006jf000537, 2007.
- 644 [15] D'Alpaos, A.: The mutual influence of biotic and abiotic components on the long-term  
645 ecomorphodynamic evolution of salt-marsh ecosystems, *Geomorphology*, 126, 269-278,  
646 10.1016/j.geomorph.2010.04.027, 2011.
- 647 [16] D'Alpaos, A., Mudd, S. M., and Carniello, L.: Dynamic response of marshes to perturbations in  
648 suspended sediment concentrations and rates of relative sea level rise, *J Geophys Res-Earth*, 116, Artn  
649 F04020, 10.1029/2011jf002093, 2011.
- 650 [17] Doody, J. P.: Coastal squeeze and managed realignment in southeast England, does it tell us anything  
651 about the future?, *Ocean Coast Manage*, 79, 34-41, 10.1016/j.ocecoaman.2012.05.008, 2013.
- 652 [18] Fagherazzi, S., Kirwan, M. L., Mudd, S. M., Guntenspergen, G. R., Temmerman, S., D'Alpaos, A., van  
653 de Koppel, J., Rybczyk, J. M., Reyes, E., Craft, C., and Clough, J.: Numerical Models of Salt Marsh  
654 Evolution: Ecological, Geomorphic, and Climatic Factors, *Rev Geophys*, 50, Artn Rg1002,  
655 10.1029/2011rg000359, 2012.
- 656 [19] Ganju, N. K., Kirwan, M. L., Dickhudt, P. J., Guntenspergen, G. R., Cahoon, D. R., and Kroeger, K. D.:  
657 Sediment transport-based metrics of wetland stability, *Geophys Res Lett*, 42, 7992-8000,  
658 10.1002/2015gl065980, 2015.
- 659 [20] Garcia, M. L., Basile, P. A., Riccardi, G. A., and Rodriguez, J. F.: Modelling extraordinary floods and  
660 sedimentological processes in a large channel-floodplain system of the Lower Parana River (Argentina),  
661 *Int J Sediment Res*, 30, 150-159, 10.1016/j.ijsrc.2015.03.007, 2015.
- 662 [21] Geselbracht, L. L., Freeman, K., Birch, A. P., Brenner, J., and Gordon, D. R.: Modeled Sea Level Rise  
663 Impacts on Coastal Ecosystems at Six Major Estuaries on Florida's Gulf Coast: Implications for  
664 Adaptation Planning, *Plos One*, 10, ARTN e0132079, 10.1371/journal.pone.0132079, 2015.
- 665 [22] Gibson, R., Atkinson, R., Gordon, J., Editors, T., In, F., Airoidi, L., and Beck, M.: Loss, Status and  
666 Trends for Coastal Marine Habitats of Europe, *An Annual Review*, 45, 345-405,  
667 10.1201/9781420050943.ch7, 2007.
- 668 [23] Horton, B. P., Shennan, I., Bradley, S. L., Cahill, N., Kirwan, M., Kopp, R. E., and Shaw, T. A.:  
669 Predicting marsh vulnerability to sea-level rise using Holocene relative sea-level data, *Nat Commun*, 9,  
670 ARTN 2687, 10.1038/s41467-018-05080-0, 2018.

- 671 [24] Howe, A. J., Rodriguez, J. F., and Saco, P. M.: Surface evolution and carbon sequestration in disturbed  
672 and undisturbed wetland soils of the Hunter estuary, southeast Australia, *Estuar Coast Shelf S*, 84, 75-  
673 83, 10.1016/j.ecss.2009.06.006, 2009.
- 674 [25] Hunt, S., Bryan, K. R., and Mullarney, J. C.: The influence of wind and waves on the existence of stable  
675 intertidal morphology in meso-tidal estuaries, *Geomorphology*, 228, 158-174,  
676 10.1016/j.geomorph.2014.09.001, 2015.
- 677 [26] Kirwan, M. L., and Murray, A. B.: A coupled geomorphic and ecological model of tidal marsh evolution,  
678 *P Natl Acad Sci USA*, 104, 6118-6122, 10.1073/pnas.0700958104, 2007.
- 679 [27] Kirwan, M. L., and Guntenspergen, G. R.: Influence of tidal range on the stability of coastal marshland,  
680 *J Geophys Res-Earth*, 115, Artn F02009, 10.1029/2009jf001400, 2010.
- 681 [28] Kirwan, M. L., Guntenspergen, G. R., D'Alpaos, A., Morris, J. T., Mudd, S. M., and Temmerman, S.:  
682 Limits on the adaptability of coastal marshes to rising sea level, *Geophys Res Lett*, 37, Artn L23401,  
683 10.1029/2010gl045489, 2010.
- 684 [29] Kirwan, M. L., and Megonigal, J. P.: Tidal wetland stability in the face of human impacts and sea-level  
685 rise, *Nature*, 504, 53-60, 10.1038/nature12856, 2013.
- 686 [30] Kirwan, M. L., Temmerman, S., Skeeahan, E. E., Guntenspergen, G. R., and Fagherazzi, S.:  
687 Overestimation of marsh vulnerability to sea level rise, *Nat Clim Change*, 6, 253-260,  
688 10.1038/Nclimate2909, 2016a.
- 689 [31] Kirwan, M. L., Walters, D. C., Reay, W. G., and Carr, J. A.: Sea level driven marsh expansion in a  
690 coupled model of marsh erosion and migration, *Geophys Res Lett*, 43, 4366-4373,  
691 10.1002/2016gl068507, 2016b.
- 692 [32] Krauss, K. W., Cahoon, D. R., Allen, J. A., Ewel, K. C., Lynch, J. C., and Cormier, N.: Surface Elevation  
693 Change and Susceptibility of Different Mangrove Zones to Sea-Level Rise on Pacific High Islands of  
694 Micronesia, *Ecosystems*, 13, 129-143, 10.1007/s10021-009-9307-8, 2010.
- 695 [33] Krone, R. B.: Flume studies of the transport of sediment in estuarial shoaling processes: Final report,  
696 University of California, Berkeley, CA, 1962.
- 697 [34] Lalimi, Y., Marani, M., Heffernan, J. B., D'Alpaos, A., and Murray, A. B.: Watershed and ocean controls  
698 of salt marsh extent and resilience, *Earth Surf Proc Land*, n/a, 10.1002/esp.4817, 2020.
- 699 [35] Larsen, L. G., Harvey, J. W., and Crimaldi, J. P.: Predicting bed shear stress and its role in sediment  
700 dynamics and restoration potential of the Everglades and other vegetated flow systems, *Ecol Eng*, 35,  
701 1773-1785, <https://doi.org/10.1016/j.ecoleng.2009.09.002>, 2009.
- 702 [36] Leong, R. C., Friess, D. A., Crase, B., Lee, W. K., and Webb, E. L.: High-resolution pattern of mangrove  
703 species distribution is controlled by surface elevation, *Estuar Coast Shelf S*, 202, 185-192,  
704 10.1016/j.ecss.2017.12.015, 2018.
- 705 [37] Lovelock, C. E., Adame, M. F., Bennion, V., Hayes, M., Reef, R., Santini, N., and Cahoon, D. R.: Sea  
706 level and turbidity controls on mangrove soil surface elevation change, *Estuar Coast Shelf S*, 153, 1-9,  
707 10.1016/j.ecss.2014.11.026, 2015a.
- 708 [38] Lovelock, C. E., Cahoon, D. R., Friess, D. A., Guntenspergen, G. R., Krauss, K. W., Reef, R., Rogers,  
709 K., Saunders, M. L., Sidik, F., Swales, A., Saintilan, N., Thuyen, L. X., and Triet, T.: The vulnerability  
710 of Indo-Pacific mangrove forests to sea-level rise, *Nature*, 526, 559-U217, 10.1038/nature15538, 2015b.
- 711 [39] Manda, A. K., Giuliano, A. S., and Allen, T. R.: Influence of artificial channels on the source and extent  
712 of saline water intrusion in the wind tide dominated wetlands of the southern Albemarle estuarine system  
713 (USA), *Environ Earth Sci*, 71, 4409-4419, 10.1007/s12665-013-2834-9, 2014.
- 714 [40] Mehta, A. J., and McAnally, W. H.: Chapter 4: Fine-grained sediment transport, in: *Sedimentation  
715 Engineering: Processes, Management, Modeling and Practice*, edited by: Garcia, M. H., ASCE manuals  
716 and reports on engineering practice, Reston, VA, 2008.
- 717 [41] Mogensen, L. A., and Rogers, K.: Validation and Comparison of a Model of the Effect of Sea-Level Rise  
718 on Coastal Wetlands, *Sci Rep-Uk*, 8, ARTN 1369, 10.1038/s41598-018-19695-2, 2018.
- 719 [42] Morris, J. T., Sundareshwar, P. V., Nietch, C. T., Kjerfve, B., and Cahoon, D. R.: Responses of coastal  
720 wetlands to rising sea level, *Ecology*, 83, 2869-2877, Doi 10.2307/3072022, 2002.

- 721 [43] Morris, J. T., Porter, D., Neet, M., Noble, P. A., Schmidt, L., Lapine, L. A., and Jensen, J. R.: Integrating  
722 LIDAR elevation data, multi-spectral imagery and neural network modelling for marsh characterization,  
723 *Int J Remote Sens*, 26, 5221-5234, Doi 10.1080/01431160500219018, 2005.
- 724 [44] Mudd, S. M., Howell, S. M., and Morris, J. T.: Impact of dynamic feedbacks between sedimentation,  
725 sea-level rise, and biomass production on near-surface marsh stratigraphy and carbon accumulation,  
726 *Estuar Coast Shelf S*, 82, 377-389, 10.1016/j.ecss.2009.01.028, 2009.
- 727 [45] Oliver, T. S. N., Rogers, K., Chafer, C. J., and Woodroffe, C. D.: Measuring, mapping and modelling:  
728 an integrated approach to the management of mangrove and saltmarsh in the Minnamurra River estuary,  
729 southeast Australia, *Wetl Ecol Manag*, 20, 353-371, 10.1007/s11273-012-9258-2, 2012.
- 730 [46] Reef, R., Schuerch, M., Christie, E. K., Moller, I., and Spencer, T.: The effect of vegetation height and  
731 biomass on the sediment budget of a European saltmarsh, *Estuar Coast Shelf S*, 202, 125-133,  
732 10.1016/j.ecss.2017.12.016, 2018.
- 733 [47] Riccardi, G.: A cell model for hydrological-hydraulic modeling, *Journal of Environmental Hydrology*,  
734 8, 1-13, 2000.
- 735 [48] Rodriguez, A. B., McKee, B. A., Miller, C. B., Bost, M. C., and Atencio, A. N.: Coastal sedimentation  
736 across North America doubled in the 20(th) century despite river dams, *Nat Commun*, 11,  
737 10.1038/s41467-020-16994-z, 2020.
- 738 [49] Rodriguez, J. F., Saco, P. M., Sandi, S., Saintilan, N., and Riccardi, G.: Potential increase in coastal  
739 wetland vulnerability to sea-level rise suggested by considering hydrodynamic attenuation effects, *Nat*  
740 *Commun*, 8, ARTN 16094, 10.1038/ncomms16094, 2017.
- 741 [50] Rogers, K., Wilton, K. M., and Saintilan, N.: Vegetation change and surface elevation dynamics in  
742 estuarine wetlands of southeast Australia, *Estuar Coast Shelf S*, 66, 559-569, 10.1016/j.ecss.2005.11.004,  
743 2006.
- 744 [51] Rogers, K., Saintilan, N., and Copeland, C.: Modelling wetland surface elevation dynamics and its  
745 application to forecasting the effects of sea-level rise on estuarine wetlands, *Ecol Model*, 244, 148-157,  
746 10.1016/j.ecolmodel.2012.06.014, 2012.
- 747 [52] Rogers, K., Saintilan, N., Howe, A. J., and Rodriguez, J. F.: Sedimentation, elevation and marsh  
748 evolution in a southeastern Australian estuary during changing climatic conditions, *Estuar Coast Shelf*  
749 *S*, 133, 172-181, 10.1016/j.ecss.2013.08.025, 2013.
- 750 [53] Saco, P., and Rodríguez, J.: Modeling Ecogeomorphic Systems, in: *Treatise on Geomorphology*, edited  
751 by: Shroder, J. F., Elsevier Inc., San Diego, 201-220, 2013.
- 752 [54] Saco, P. M., Rodríguez, J. F., Moreno-de las Heras, M., Keesstra, S., Azadi, S., Sandi, S., Baartman, J.,  
753 Rodrigo-Comino, J., and Rossi, J.: Using hydrological connectivity to detect transitions and degradation  
754 thresholds: Applications to dryland systems, *Catena*, 186, 10.1016/j.catena.2019.104354, 2019.
- 755 [55] Saintilan, N., Wilson, N. C., Rogers, K., Rajkaran, A., and Krauss, K. W.: Mangrove expansion and salt  
756 marsh decline at mangrove poleward limits, *Global Change Biol*, 20, 147-157, 10.1111/gcb.12341, 2014.
- 757 [56] Saintilan, N., Khan, N. S., Ashe, E., Kelleway, J. J., Rogers, K., Woodroffe, C. D., and Horton, B. P.:  
758 Thresholds of mangrove survival under rapid sea level rise, *Science*, 368, 1118-+, ARTN aba2656,  
759 10.1126/science.aba2656, 2020.
- 760 [57] Sandi, S. G., Rodriguez, J. F., Saintilan, N., Riccardi, G., and Saco, P. M.: Rising tides, rising gates: The  
761 complex ecogeomorphic response of coastal wetlands to sea-level rise and human interventions, *Adv*  
762 *Water Resour*, 114, 135-148, 10.1016/j.advwatres.2018.02.006, 2018.
- 763 [58] Sandi, S. G., Saco, P. M., Saintilan, N., Wen, L., Riccardi, G., Kuczera, G., Willgoose, G., and Rodriguez,  
764 J. F.: Detecting inundation thresholds for dryland wetland vulnerability, *Adv Water Resour*, 128, 168-  
765 182, 10.1016/j.advwatres.2019.04.016, 2019.
- 766 [59] Sandi, S. G., Rodriguez, J. F., Saintilan, N., Wen, L., Kuczera, G., Riccardi, G., and Saco, P. M.:  
767 Resilience to drought of dryland wetlands threatened by climate change, *Sci Rep-Uk*,  
768 <https://doi.org/10.1038/s41598-020-70087-x>, 2020a.
- 769 [60] Sandi, S. G., Saco, P. M., Rodriguez, J. F., Saintilan, N., Wen, L., Kuczera, G., Riccardi, G., and  
770 Willgoose, G.: Patch organization and resilience of dryland wetlands, *Sci Total Environ*, 726, ARTN  
771 138581, 10.1016/j.scitotenv.2020.138581, 2020b.

- 772 [61] Schuerch, M., Spencer, T., Temmerman, S., Kirwan, M. L., Wolff, C., Lincke, D., McOwen, C. J.,  
773 Pickering, M. D., Reef, R., Vafeidis, A. T., Hinkel, J., Nicholls, R. J., and Brown, S.: Future response of  
774 global coastal wetlands to sea-level rise, *Nature*, 561, 231-+, 10.1038/s41586-018-0476-5, 2018.
- 775 [62] Silvestri, S., Defina, A., and Marani, M.: Tidal regime, salinity and salt marsh plant zonation, *Estuar*  
776 *Coast Shelf S*, 62, 119-130, 10.1016/j.eess.2004.08.010, 2005.
- 777 [63] Tabak, N. M., Laba, M., and Spector, S.: Simulating the Effects of Sea Level Rise on the Resilience and  
778 Migration of Tidal Wetlands along the Hudson River, *Plos One*, 11, ARTN e0152437,  
779 10.1371/journal.pone.0152437, 2016.
- 780 [64] Temmerman, S., Govers, G., Wartel, S., and Meire, P.: Spatial and temporal factors controlling short-  
781 term sedimentation in a salt and freshwater tidal marsh, Scheldt estuary, Belgium, SW Netherlands, *Earth*  
782 *Surf Proc Land*, 28, 739-755, 10.1002/esp.495, 2003.
- 783 [65] Temmerman, S., Bouma, T. J., Govers, G., Wang, Z. B., De Vries, M. B., and Herman, P. M. J.: Impact  
784 of vegetation on flow routing and sedimentation patterns: Three-dimensional modeling for a tidal marsh,  
785 *J Geophys Res-Earth*, 110, Artn F04019, 10.1029/2005jf000301, 2005.
- 786 [66] Temmerman, S., Moonen, P., Schoelynck, J., Govers, G., and Bouma, T. J.: Impact of vegetation die-off  
787 on spatial flow patterns over a tidal marsh, *Geophys Res Lett*, 39, Artn L03406, 10.1029/2011gl050502,  
788 2012.
- 789 [67] Temmerman, S., and Kirwan, M. L.: Building land with a rising sea, *Science*, 349, 588-589,  
790 10.1126/science.aac8312, 2015.
- 791 [68] Thorne, J. H., Choe, H., Stine, P. A., Chambers, J. C., Holguin, A., Kerr, A. C., and Schwartz, M. W.:  
792 Climate change vulnerability assessment of forests in the Southwest USA, *Climatic Change*, 148, 387-  
793 402, 10.1007/s10584-017-2010-4, 2018.
- 794 [69] Tian, B., Wu, W. T., Yang, Z. Q., and Zhou, Y. X.: Drivers, trends, and potential impacts of long-term  
795 coastal reclamation in China from 1985 to 2010, *Estuar Coast Shelf S*, 170, 83-90,  
796 10.1016/j.eess.2016.01.006, 2016.
- 797 [70] Van Loon-Steensma, J. M., Van Dobben, H. F., Slim, P. A., Huiskes, H. P. J., and Dirkse, G. M.: Does  
798 vegetation in restored salt marshes equal naturally developed vegetation?, *Appl Veg Sci*, 18, 674-682,  
799 10.1111/avsc.12182, 2015.
- 800 [71] Williams, R. J., and Watford, F. A.: Identification of structures restricting tidal flow in New South Wales,  
801 Australia, *Wetl Ecol Manag*, 5, 87-97, 10.1023/A:1008283522167, 1997.
- 802 [72] Woodroffe, C. D., Rogers, K., McKee, K. L., Lovelock, C. E., Mendelssohn, I. A., and Saintilan, N.:  
803 Mangrove Sedimentation and Response to Relative Sea-Level Rise, *Annu Rev Mar Sci*, 8, 243-266,  
804 10.1146/annurev-marine-122414-034025, 2016.
- 805



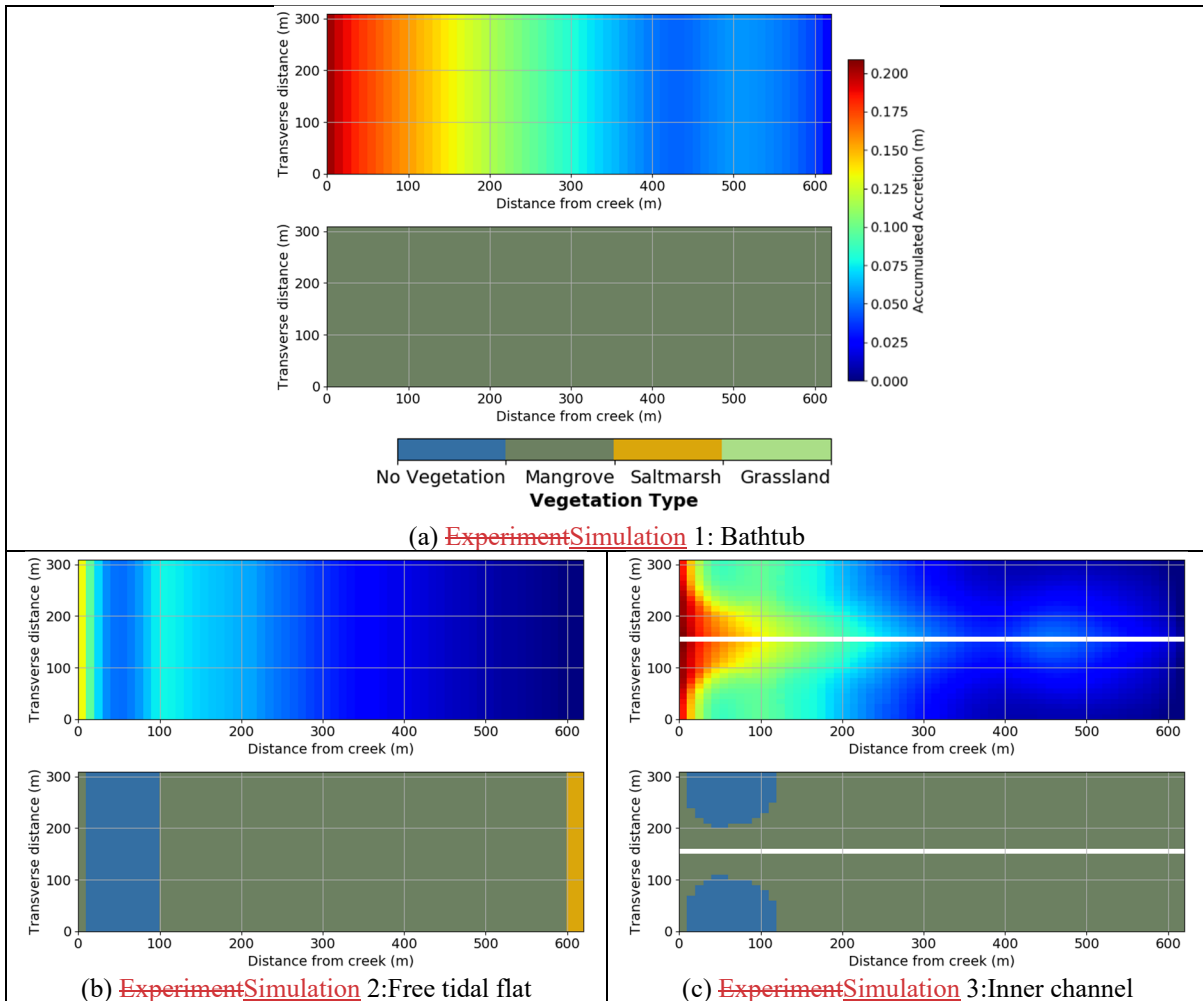
807 Figure 1. Field site and areas within the site characterised by the numerical ~~experiments~~simulations: a) Area E of  
 808 Kooragang wetlands, b) areas within the wetland where the simplified ~~experiments~~simulations represent the dominant  
 809 processes, c) ~~schematic longitudinal view of the domain setup and sinusoidal wave input (a~~Adapted from Rodriguez et  
 810 ~~al. (2017), ed) schematic of the experimental setup corresponding to Experiment 2. The other experiments have a~~  
 811 ~~similar setup but incorporate more local features like an internal drainage channel and an embankment with a~~  
 812 ~~culvert~~isometric view of each simulated domain and their hydraulic features. Vegetation cover is only indicative and  
 813 ~~roughly corresponds to early stages of the simulations. Elevation unit, mAMSL, stands for metres above mean sea level.~~  
 814 ~~Adapted from Rodriguez et al. (2017)~~

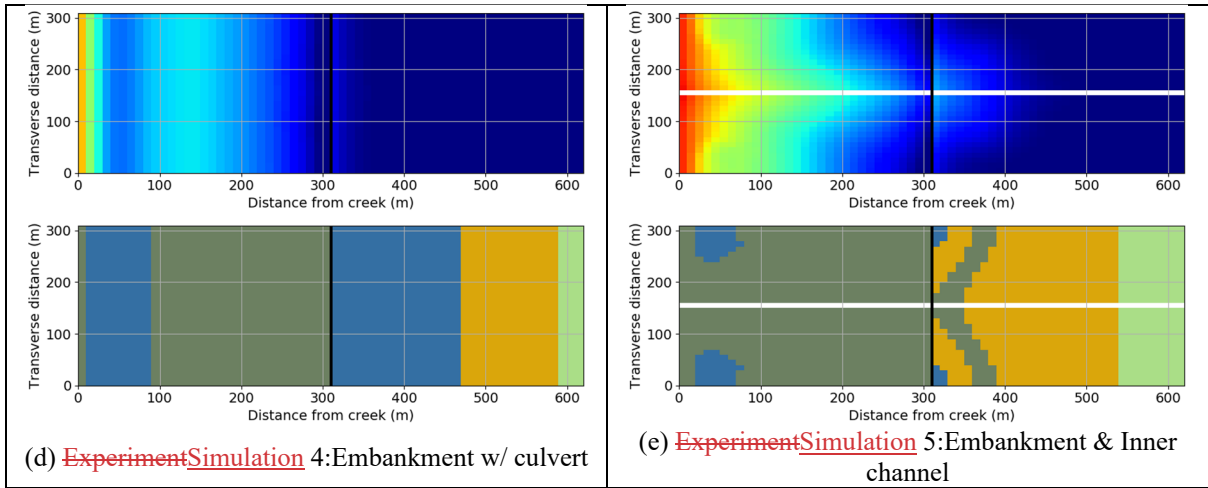
815 Table 1: Parameters of soil surface elevation model

Model Parameter	Mangrove	Saltmarsh
$a$ (g/m <sup>4</sup> )	-6,037.6	-16,767
$b$ (g/m <sup>3</sup> )	7,848.9	8,384
$c$ (g/m <sup>2</sup> )	-1,328.3	0
$q$ (m <sup>3</sup> /year/g)	$9 \times 10^{-5}$	$9 \times 10^{-5}$
$k$ (m <sup>5</sup> /g <sup>2</sup> )	$1.2 \times 10^{-7}$	$6.2 \times 10^{-7}$

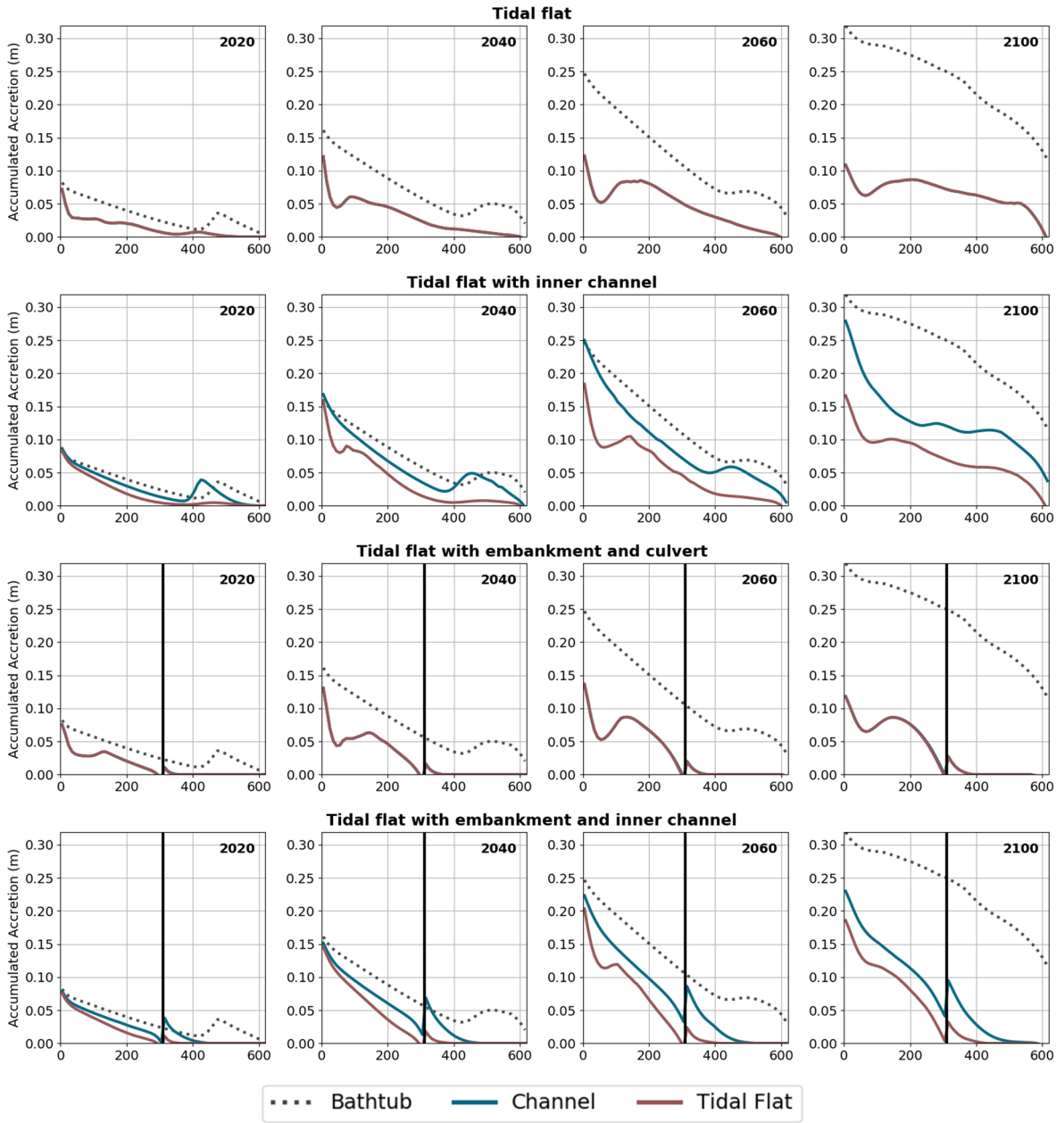
816

817





818 **Figure 2. Accumulated accretion (top) and vegetation maps (bottom) in 2050 for low sediment input corresponding to:**  
 819 **a) ExperimentSimulation 1, b) ExperimentSimulation 2, c) ExperimentSimulation 3, d) ExperimentSimulation 4, e)**  
 820 **ExperimentSimulation 5.**



821

822

823

824

825

826

827

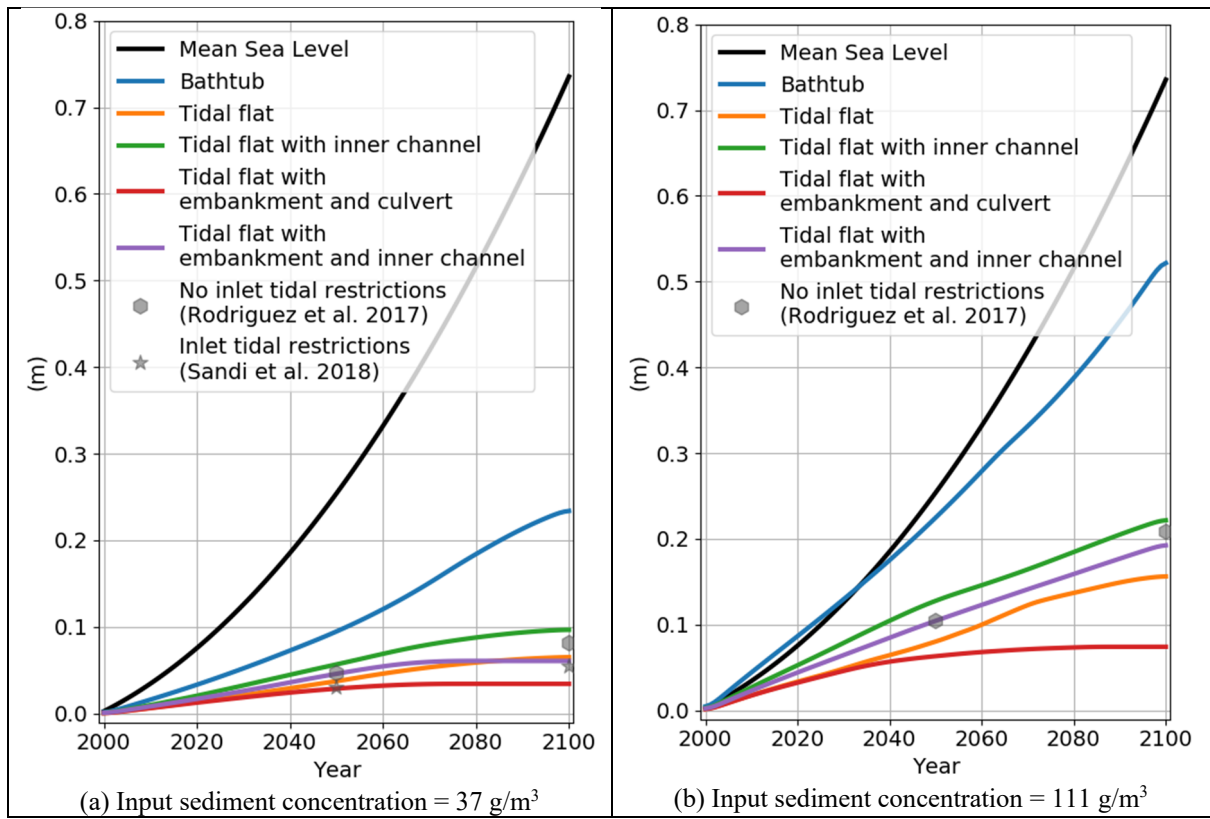
828

829

830

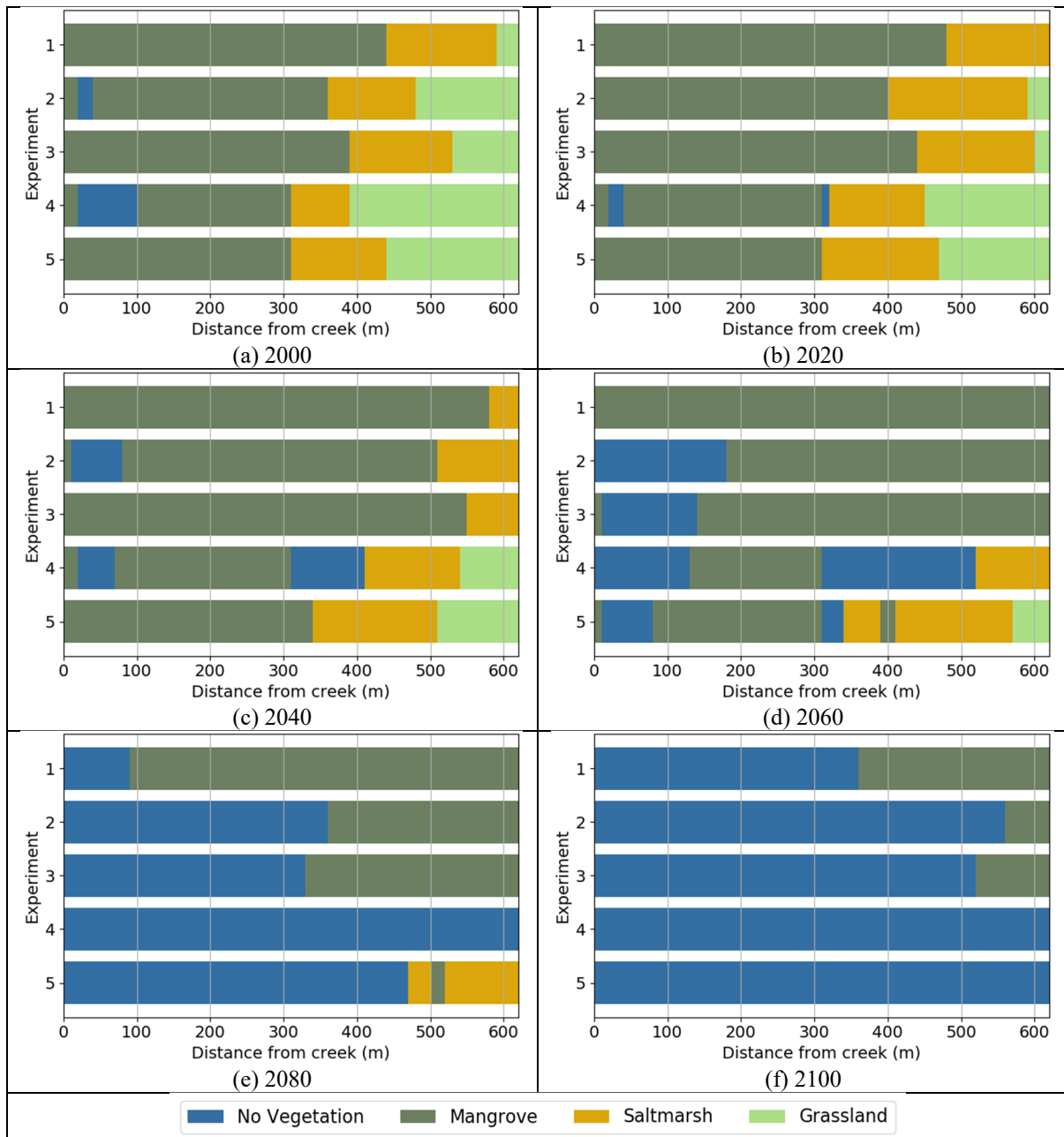
Figure 3. Longitudinal profiles of accumulated accretion ( $\Delta E$ , m) for a sediment supply of  $37 \text{ g/m}^3$ . The vertical black line represents the embankment with culvert. The “channel” profile represents the elevation gain near the central channel, while the “tidal flat” profile is situated in the middle of the tidal flat. Note: simulation starts in the year 2000.





831 Figure 4. Sea-Level Rise and domain-average accumulated accretion over time for all simulation experiments for a)  
 832 low sediment input and b) high sediment input. Results from Rodriguez et al. (2017) and Sandi et al. (2018)  
 833 corresponding to the entire Area E wetland are included for comparison.

834  
 835  
 836  
 837  
 838  
 839  
 840  
 841  
 842  
 843  
 844  
 845  
 846

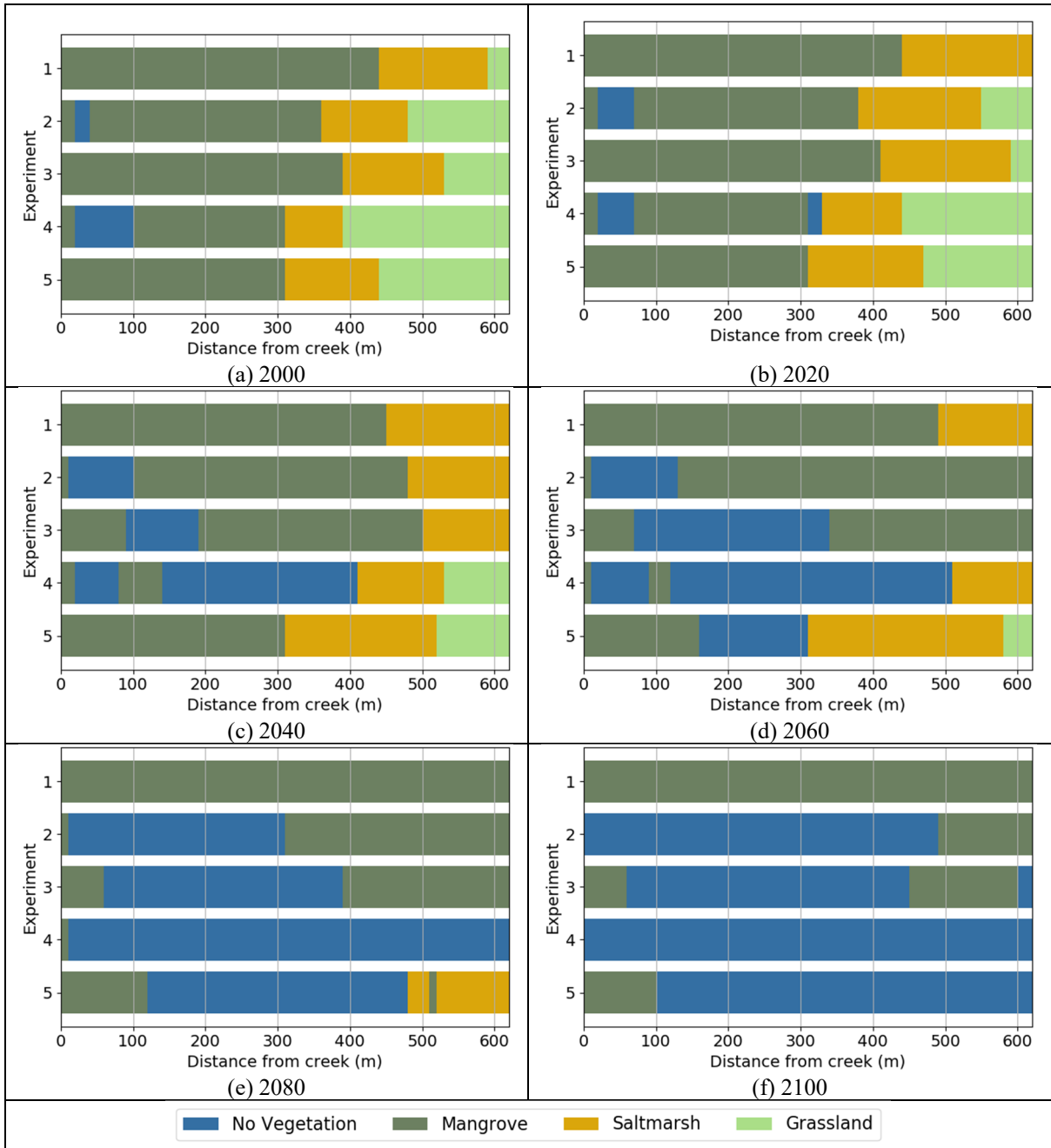


847 **Figure 5. Predominant position occupied by each vegetation type in the tidal flat from 2000 to 2100. Simulations for low**  
 848 **sediment input,  $SSC = 37 \text{ g/m}^3$ . Experiments: 1 Bathtub, 2 Free tidal flat, 3 Inner channel, 4 Embankment with culvert**  
 849 **and 5 Embankment and inner channel.**

850

851

852

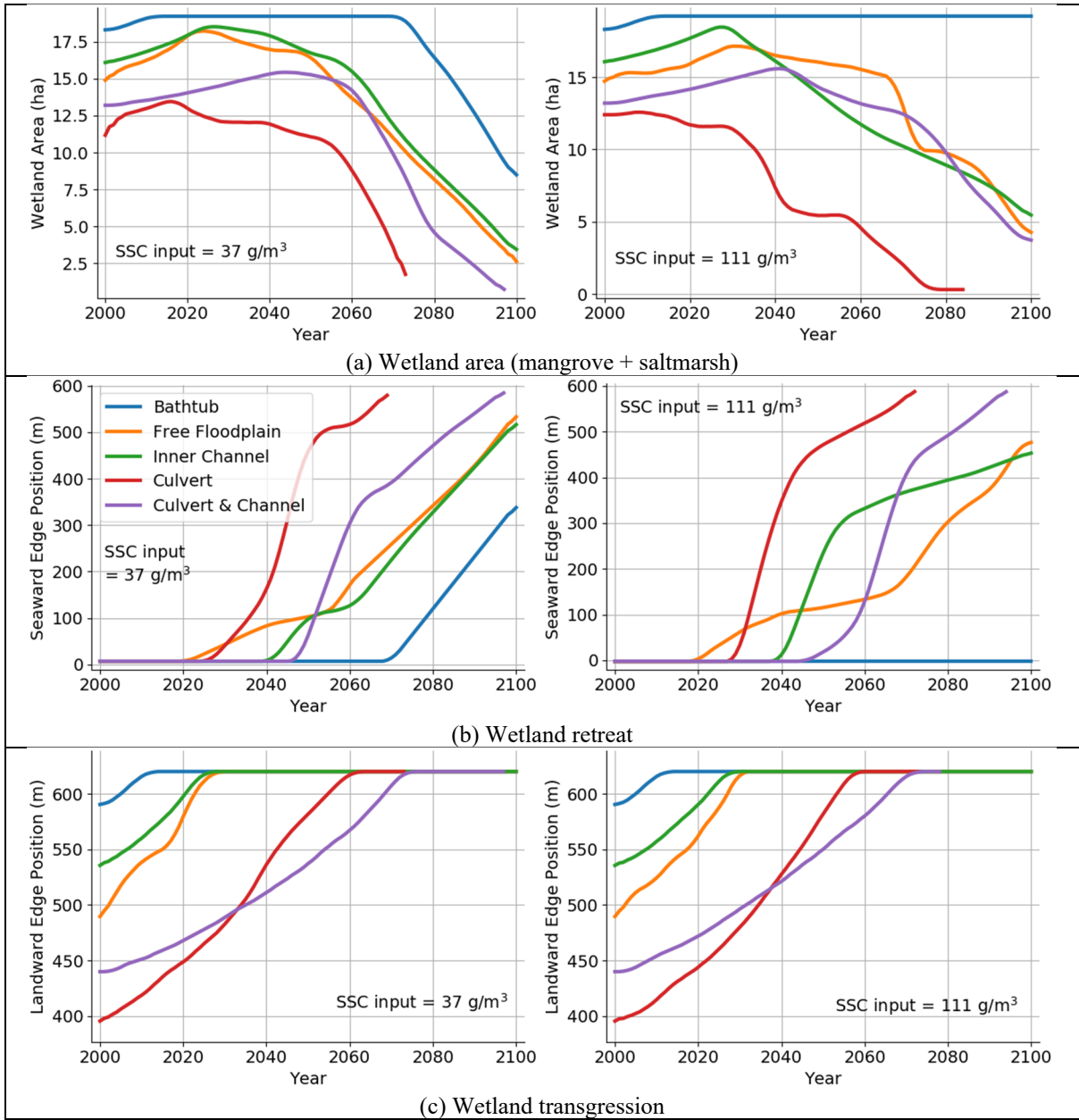


853 **Figure 6. Predominant position occupied by each vegetation type in the tidal flat from 2000 to 2100. Simulations for**  
 854 **high sediment input,  $SSC = 111 \text{ g/m}^3$ . Experiments: 1 Bathtub, 2 Free tidal flat, 3 Inner channel, 4 Embankment with**  
 855 **culvert and 5 Embankment and inner channel.**

856

857

858



859 **Figure 7. Time evolution of wetland in poor (SSC=37 g/m<sup>3</sup>) and rich (SSC=111 g/m<sup>3</sup>) sediment environments under**  
 860 **SLR. a) wetland area; b) wetland retreat and; c) wetland transgression**

861

862

863